






ARTICLE

The exocyst controls lysosome secretion and antigen extraction at the immune synapse of B cells

Juan José Sáez^{1,2} , Jheimmy Diaz¹, Jorge Ibañez¹, Juan Pablo Bozo¹, Fernanda Cabrera Reyes¹, Martina Alamo¹, François-Xavier Gobert³, Dorian Obino³ , María Rosa Bono² , Ana-María Lennon-Duménil³, Charles Yeaman⁴ , and María-Isabel Yuseff¹ 

B lymphocytes capture antigens from the surface of presenting cells by forming an immune synapse. Local secretion of lysosomes, which are guided to the synaptic membrane by centrosome repositioning, can facilitate the extraction of immobilized antigens. However, the molecular basis underlying their delivery to precise domains of the plasma membrane remains elusive. Here we show that microtubule stabilization, triggered by engagement of the B cell receptor, acts as a cue to release centrosome-associated Exo70, which is redistributed to the immune synapse. This process is coupled to the recruitment and activation of GEF-H1, which is required for assembly of the exocyst complex, used to promote tethering and fusion of lysosomes at the immune synapse. B cells silenced for GEF-H1 or Exo70 display defective lysosome secretion, which results in impaired antigen extraction and presentation. Thus, centrosome repositioning coupled to changes in microtubule stability orchestrates the spatial-temporal distribution of the exocyst complex to promote polarized lysosome secretion at the immune synapse.

Introduction

B lymphocytes display the unique ability to mount antibody responses against invading pathogens. To achieve this function, they must capture external antigens and present them as peptide fragments loaded onto major histocompatibility complex class II (MHC-II) molecules to CD4⁺ T cells, which in turn provide the necessary signals for B cells to become fully activated (Mitchison, 2004; Avalos and Ploegh, 2014). In vivo, B cells predominantly recognize and capture antigens tethered at the surface of other presenting cells by forming a transient polarized domain known as the immune synapse (IS). B cells use this platform to focus signaling networks as well as to recruit specialized molecules involved in antigen internalization and processing (Carrasco et al., 2004; Natkanski et al., 2013; Heesters et al., 2016).

Early events of IS assembly, initiated by the B cell receptor (BCR) engagement with surface-tethered antigens, involve rapid actin cytoskeleton rearrangements, which act in concert with the microtubule network to promote the gathering of antigens toward the center of the synapse (Lin et al., 2008; Treanor et al., 2010; Harwood and Batista, 2011; Mattila et al., 2013). Antigens are further internalized by the use of mechanical forces exerted

by Myosin IIA at the synaptic membrane (Natkanski et al., 2013) or by enzymatic extraction, which relies on hydrolases released by the local secretion of MHC-II⁺ lysosomes at the IS (Yuseff et al., 2011, 2013). Analogously to observations made in cytotoxic T cells and natural killer (NK) cells, the recruitment of lysosomes to the IS of B cells is guided by repositioning of the microtubule-organizing center or centrosome (Stinchcombe et al., 2006; Stinchcombe and Griffiths, 2007; Orange, 2008), where polarity proteins such as aPKC/Cdc42 and Par3 play a critical role (Yuseff et al., 2011; Reversat et al., 2015). Thus, directional secretion at the IS enables B lymphocytes to perform effector functions and emerges as an interesting model to study polarized membrane trafficking.

To understand how lysosome secretion is coupled to centrosome repositioning, we hypothesized that this non-membranous organelle could harbor effector molecules that regulate polarized membrane trafficking at the IS. A proteomic analysis from isolated centrosome fractions obtained from B cells (Obino et al., 2016) revealed that four subunits belonging to the exocyst complex, Sec3, Sec5, Sec8, and Exo70, were enriched at this level. The exocyst is an evolutionarily conserved

¹Department of Cellular and Molecular Biology, Faculty of Sciences, Pontificia Universidad Católica de Chile, Santiago, Chile; ²Department of Biology, Faculty of Sciences, Universidad de Chile, Santiago, Chile; ³INSERM U932, Institut Curie, Centre de Recherche, PSL Research University, Paris, Île-de-France, France; ⁴Department of Anatomy and Cell Biology, University of Iowa, Iowa City, IA.

Correspondence to María-Isabel Yuseff: myuseff@bio.puc.cl; D. Obino's present address is Pathogenesis of vascular infections unit, INSERM U1225, Institut Pasteur, Paris, France.

© 2019 Sáez et al. This article is distributed under the terms of an Attribution–Noncommercial–Share Alike–No Mirror Sites license for the first six months after the publication date (see <http://www.rupress.org/terms/>). After six months it is available under a Creative Commons License (Attribution–Noncommercial–Share Alike 4.0 International license, as described at <https://creativecommons.org/licenses/by-nc-sa/4.0/>).

hetero-oligomer comprising eight proteins: Sec3, Sec5, Sec6, Sec8, Sec10, Sec15, Exo70, and Exo84. This complex functions as an anchoring component to target secretory vesicles to precise domains of the plasma membrane, thereby promoting their local secretion (Zeng et al., 2017). Initial observations in budding yeast revealed that silencing of different exocyst subunits generates defects in secretion (Novick et al., 1980; TerBush et al., 1996). In polarized epithelial cells, the exocyst regulates vesicle trafficking to different membrane domains and is implicated in the assembly and stability of cellular junctions (Grindstaff et al., 1998; Lipschutz et al., 2000; Polgar and Fogelgren, 2018). Recent reports also highlight additional cellular processes where the exocyst is involved, such as cell invasion, membrane protrusion, and autophagy (Spiczka and Yeaman, 2008; Liu et al., 2009; Bodemann et al., 2011; Thapa et al., 2012; Yamamoto et al., 2013). Thus, the assembly of exocyst components within specific domains of the cell regulates a wide range of functions; however, the mechanisms that control its assembly and recruitment to membrane domains are poorly understood.

In this work, we used B lymphocytes to explore the role of the exocyst in polarized lysosome trafficking at the IS and associated mechanisms involved. Our work reveals that BCR engagement promotes the stabilization of the microtubule network associated to the centrosome. This acts as a cue to release centrosome-associated Exo70, thereby favoring its recruitment to the IS. Additionally, BCR stimulation triggers the activation of GTP exchange factor H1 (GEF-H1), which dissociates from microtubules upon activation and is involved in exocyst assembly. Accordingly, we show that GEF-H1 accumulates at the synaptic membrane of activated B cells and is required for the assembly of the exocyst complex. Both Exo70 and GEF-H1 are necessary to promote the stable docking and subsequent fusion of lysosomes at the IS, which facilitates the extraction and presentation of immobilized antigens. Together, these results unveil a mechanistic link between microtubule dynamics and spatial-temporal regulation of polarized lysosome secretion.

Results

BCR stimulation triggers the recruitment of exocyst subunits to the IS and complex assembly

The interaction of B cells with immobilized antigens triggers the formation of an IS, where centrosome repositioning orchestrates the stable recruitment of lysosomes. To understand the molecular mechanisms behind this process, we searched for centrosome-associated proteins that could regulate lysosome trafficking. A proteomic analysis previously performed of isolated centrosomes obtained from activated and resting mouse B lymphoma cells (Obino et al., 2016) revealed that four of the eight exocyst complex subunits, Sec3, Sec5, Sec8, and Exo70, were found at this level and became increased within these fractions upon activation (Fig. S1 A). In agreement with these data, Western blot analysis confirmed that these subunits were found in centrosome-enriched fractions (Fig. S1 B). Two of the subunits found to be associated with centrosome fractions,

Sec3 and Exo70, have been extensively studied in yeast and mammalian epithelial cells, where they bind the plasma membrane, acting as a landmark for the anchoring of secretory vesicles (He et al., 2007; Liu et al., 2007; Zhang et al., 2008; Baek et al., 2010); however, no studies have been reported on the localization and function of the exocyst complex in B cells.

Considering that we found exocyst subunits associated to the centrosome, an organelle known to guide lysosome recruitment to the IS, we sought to determine the role of the exocyst in lysosome trafficking in B cells. To evaluate whether these subunits were recruited to the synaptic membrane of activated B cells, we first performed immunofluorescence staining of endogenous Exo70 and HA-tagged Sec3 in resting and activating conditions, where B cells were activated with beads containing F(ab')₂ anti-IgG, termed BCR ligand*. This system, previously used to mimic the interaction of B cells with immobilized antigen, creates a polarized contact site, hereafter refer to as IS (Batista and Neuberger, 2000; Yuseff et al., 2011, 2013). Intriguingly, in resting B lymphocytes, Exo70 and Sec3 have different subcellular localizations. Whereas Exo70 displayed discrete perinuclear localization consistent with a centrosomal association, Sec3-HA was distributed within vesicular structures, which partially colocalized with the lysosome marker LAMP-1 (Fig. 1 A and Fig. S1, C and D). Although we cannot rule out that overexpression of Sec3-HA could lead to its mislocalization, these Sec3⁺ vesicular structures could correspond to compartments that cofractionate with the centrosome, where endogenous Sec3 was detected by immunoblot (Fig. S1 B). Noticeably, upon activation, both subunits are recruited to the IS, as confirmed by calculating their polarity indexes (a measurement of their proximity to the IS; Figs. 1 A and S1 E; Materials and methods). This process occurred concomitantly with the recruitment of LAMP-1⁺ lysosomes (Fig. 1 A). As both proteins have phospholipid-interacting domains (Dong et al., 2005; Hamburger et al., 2006; He et al., 2007; Liu et al., 2007; Moore et al., 2007), we analyzed whether they could be detected in purified synaptic membranes isolated from activated B cells. For this, B cells were activated with BCR ligand* magnetic beads for indicated times, and synaptic membrane fractions (bead-associated complexes) were isolated by magnetic interactions and their contents analyzed by immunoblot (Larghi et al., 2013). We detected an activation-dependent accumulation of LAMP-1, Exo70, and Sec3 in synaptic membranes isolated from B cells, whereas the cytosolic protein GAPDH was not detected (Fig. 1 B). We next evaluated whether the exocyst complex was assembled during B cell activation. For this purpose, Exo70 was immunoprecipitated from resting and activated B cells for different times, and association of other subunits was detected. Our results show that several components of the exocyst coimmunoprecipitated with Exo70 after 60 min of activation and significantly decreased after 120 min (Fig. 1 C), indicating that B cell activation is associated with the transient assembly of the exocyst complex. Overall, these results highlight how BCR engagement triggers the local recruitment of Exo70 and Sec3 at the IS and, concomitantly, the assembly of the exocyst complex.

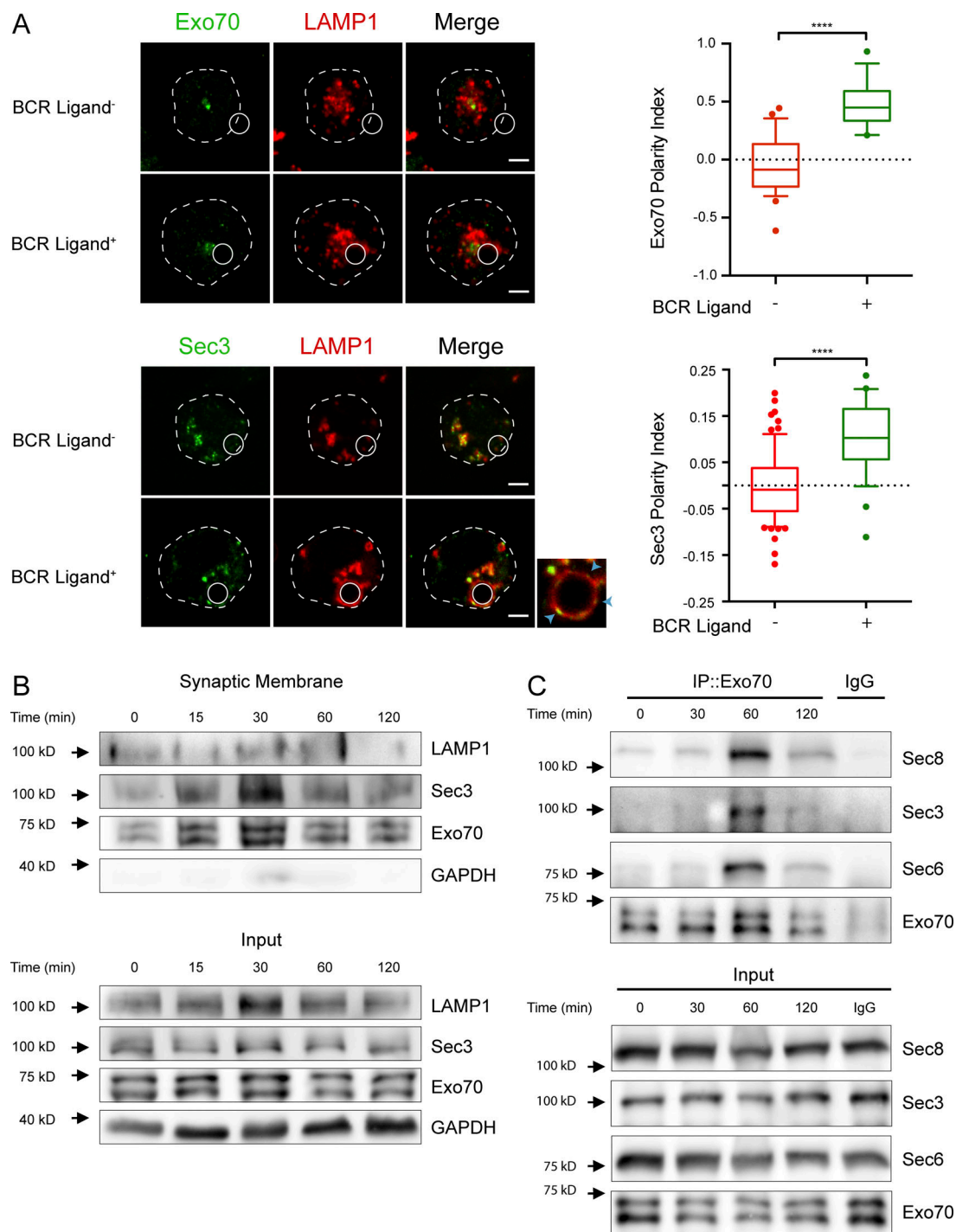


Figure 1. BCR engagement triggers the recruitment of Exo70 and Sec3 to the IS and exocyst assembly. **(A)** Left: Representative confocal images of B cells incubated with nonactivating (BCR ligand⁻) or activating (BCR ligand⁺) beads for 1 h at 37°C. Cells were fixed and stained for endogenous Exo70 (green) and LAMP-1 (red) or transfected with Sec3-HA and stained for HA (green) and LAMP-1 (red). White circles and dashed lines indicate bead position and cell boundaries, respectively. Blue arrowheads on inset point to LAMP-1⁺Sec3⁺ spots at the IS. Scale bar: 3 μ m. Right: Quantification of Exo70 or Sec3 polarity indexes toward the IS. Data are shown as box-and-whisker plots. The ends of whiskers represent the 10th and 90th percentile. Unpaired *t* test; ****, *P* < 0.0001; Exo70 polarity index was calculated from *n* ≥ 39 cells from three independent experiments; Sec3, from *n* ≥ 26 cells from two independent experiments. **(B)** B cells were stimulated with BCR ligand⁺ Dynabeads for the indicated times, and synaptic membranes were isolated containing BCR-associated protein complexes, followed by Exo70, Sec3, LAMP-1, and GAPDH detection by Western blot. Representative of two independent experiments. **(C)** Exo70 immunoprecipitation (IP) assay to detect the formation of the exocyst complex in B cells activated for indicated times. Representative of four independent experiments.

The centrosome-associated pool of Exo70 diminishes upon activation

Our results show that in B cells, Exo70 is found within centrosome fractions and is recruited to the synaptic membrane upon activation. To further characterize the recruitment of Exo70 to the IS, we determined whether its subcellular localization correlated with the positioning of the centrosome and lysosomes, which are both mobilized to the IS upon B cell activation (Yuseff et al., 2011). For this, B cells were incubated for indicated times with BCR ligand⁺ or nonactivating beads containing F(ab')₂ anti-IgM, termed BCR ligand⁻. Immunofluorescence staining of endogenous Exo70 together with the centrosome confirmed that Exo70 was concentrated closely to the centrosome (Fig. 2 A), whereas no significant staining was detected at the plasma membrane, contrasting with observations made in other cell types (He et al., 2007; Liu et al., 2007; Oztan et al., 2007; Ma et al., 2016). A similar distribution of Exo70 was observed in primary B cells isolated from mouse spleens (Fig. S2 A). Noticeably, we observed that upon BCR engagement, Exo70 was mobilized to the IS together with the centrosome (Fig. 2 A). Accordingly, polarity indexes calculated for Exo70 and the centrosome confirmed their co-recruitment to the IS upon activation with BCR ligand⁺ beads (Fig. 2 B), displaying a very strong correlation (Fig. 2 C). Of note, polarization of Exo70 and the centrosome was not observed in B cells stimulated with nonactivating beads (Fig. 2 A, lower panel), demonstrating that this process relies on BCR engagement. In addition to the previous observations, we noticed that the amount of Exo70 associated with the centrosome of B cells decreased concomitantly with its polarization to the IS (Fig. 2 A). Quantification of the concentration of Exo70 around the centrosome, and its colocalization with centrin during B cell activation, suggested that Exo70 became dissociated from the centrosome upon activation (Fig. 2, D and E). Consistent with this observation, fractionation of B cells on a “membrane flotation” density gradient revealed that BCR stimulation triggered a redistribution of Exo70 from higher to lower density fractions, which contained a bona fide membrane marker (LAMP-1), suggesting that Exo70 shifts from a microtubule-associated fraction to membrane compartments upon B cell activation (Fig. S2 C). Thus, lower levels of Exo70 at the centrosome correlate with its accumulation at the synaptic membrane (Figs. 1 B and S2 B), suggesting that BCR stimulation triggers the mobilization of Exo70 from the centrosome to the IS.

Accumulation of Exo70 at the centrosome is regulated by microtubule dynamics

We next searched for mechanisms that could control the association of Exo70 with the centrosome during B cell activation. Exo70 has been shown to directly interact with microtubules and the actin branching complex Arp2/3 (Wang et al., 2004; Zuo et al., 2006). We therefore explored whether the subcellular distribution of Exo70 relied on the integrity of the microtubule network or actin cytoskeleton, which also accumulates at the centrosome of B cells (Obino et al., 2016). No significant effects in the distribution of Exo70 were observed when disrupting the actin cytoskeleton using Latrunculin A (Fig. S3, A and B).

However, in the presence of paclitaxel, a microtubule-stabilizing drug, we observed a drastic change in the distribution of Exo70, which was no longer confined to one spot (i.e., the centrosome) and adopted a more disperse localization throughout the cytoplasm (Fig. 3 A). Quantitative analysis showed a significant decrease in the accumulation of Exo70 within a defined area (Materials and methods) when the microtubule network was stabilized by paclitaxel. No significant effect was observed in nocodazole-treated cells, where Exo70 remained accumulated at the nonpolarized centrosome (Fig. 3, A and B). Noticeably, upon activation, paclitaxel-treated B cells showed a marked accumulation of Exo70 at the site of engagement with antigen-coated beads (Fig. 3 A, middle panel), suggesting that the interaction of Exo70 with the microtubule cytoskeleton was preventing this subunit from becoming associated with the synaptic membrane.

Given that enhanced stabilization of microtubules uncoupled Exo70 from the centrosome, we hypothesized that changes in tubulin stability triggered upon B cell activation could act as a signal to dissociate Exo70 from the microtubule network, thereby allowing its recruitment to the IS. To investigate this possibility, we evaluated two parameters that could indicate increased microtubule stability at the centrosome in resting and activated B cells: (1) the amount of microtubules associated at the centrosome and (2) tubulin acetylation, a posttranslational modification associated with microtubule stability (Westermann and Weber, 2003). Imaging analysis revealed that activated B cells displayed an increase in the density of microtubules at the centrosome (Fig. 3 C), which correlated with higher levels of acetylated tubulin in this region (Fig. 3 D). Accordingly, we also detected an increase in acetylated tubulin by Western blot analysis, which was highest after 30 min of activation, at which time the centrosome is polarized at the IS (Fig. 3 E). Noticeably, by enhancing microtubule acetylation using suberoylanilide hydroxamic acid (SAHA), an inhibitor of histone deacetylase 6 (Zhang et al., 2003; Fig. S3 C), we also depleted Exo70 from the centrosome (Fig. 3 F). Overall, these results reveal that the association of Exo70 with the centrosome is regulated by microtubule stability, which is enhanced upon BCR stimulation.

GEF-H1 interacts with Exo70 during B cell synapse formation and is required for assembly of the exocyst complex

Having shown that microtubule stability regulates the subcellular localization of Exo70 in B cells, we next searched for potential regulators of the exocyst and focused on the rho activating factor GEF-H1, known to dynamically interact with microtubules and promote exocyst assembly upon activation (Krendel et al., 2002; Birkenfeld et al., 2008; Pathak et al., 2012). Interestingly, inactive GEF-H1 is found associated with microtubules, from which it is released upon activation, where it interacts with exocyst subunits and RhoA to promote exocyst functions (Krendel et al., 2002; Birkenfeld et al., 2008; Pathak and Dermardirossian, 2013). Similar to Exo70, our results show that in resting B cells, GEF-H1 accumulates at the centrosome, from which it decreases upon BCR engagement (Fig. 4 A). This result correlates with the dephosphorylation of GEF-H1 in Ser885 (Fig. 4 B), a modification needed to achieve its active

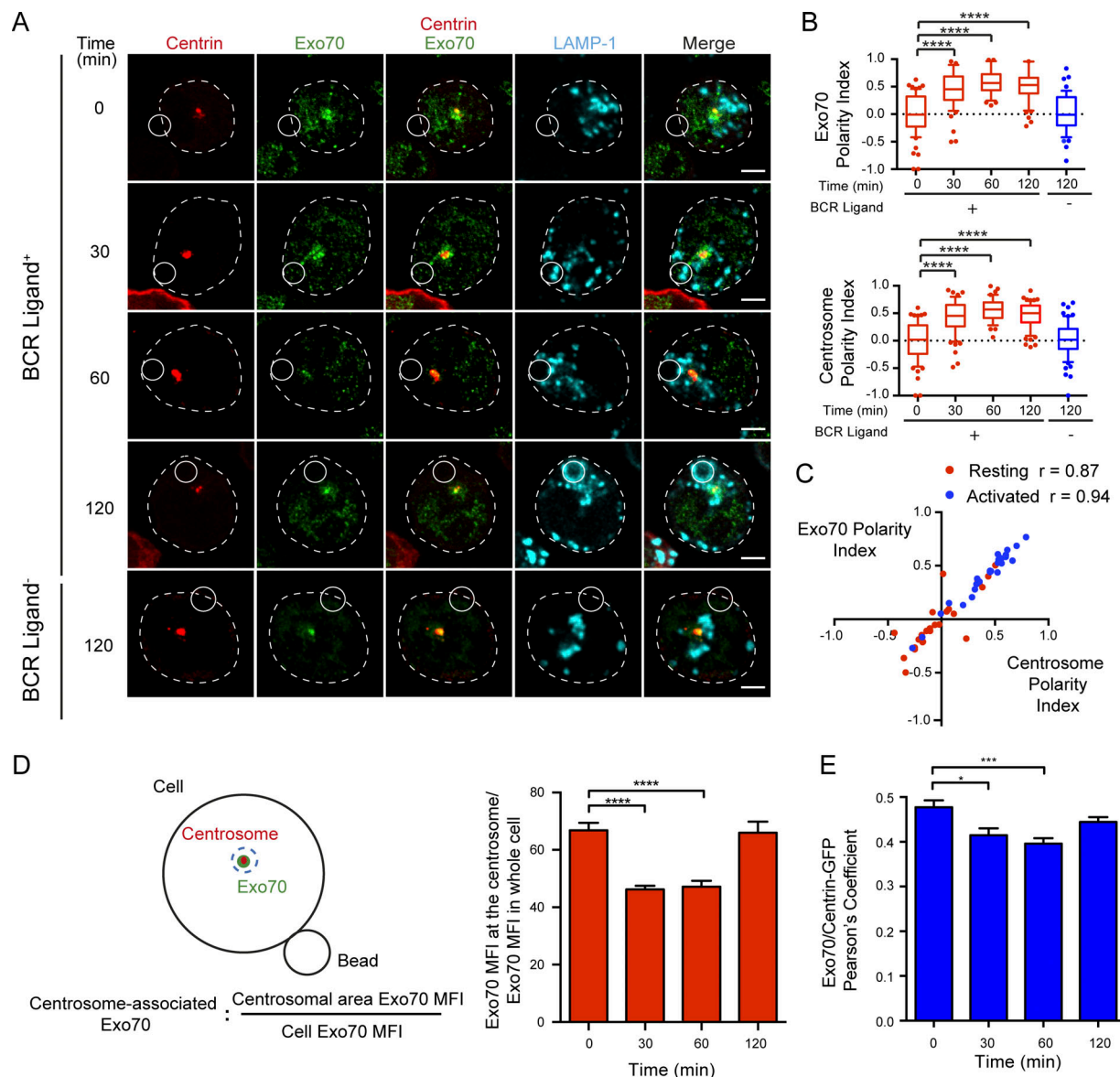


Figure 2. Exo70 is enriched at the centrosome of B cells. (A) Confocal images of centrin-GFP-expressing cells (shown in red) activated with BCR ligand-positive or -negative beads for the indicated times. Exo70 (green) and LAMP-1 (cyan). Scale bar: 3 μ m. (B) Exo70 and centrosome polarity indexes were calculated from the images in A. ****, $P < 0.0001$; two-way ANOVA with Sidak's multiple comparison test; $n \geq 39$ cells from three independent experiments. (C) Correlation analysis between Exo70 and centrosome polarity indexes from B cells resting (red) and activated for 120 min (blue). (Spearman correlation coefficient). (D) Left: Scheme depicting the method used to quantify centrosome-associated Exo70. Right: Quantification of centrosome-associated Exo70 during B cell activation. ****, $P < 0.0001$; two-way ANOVA with Sidak's multiple comparison test; $n \geq 64$ cells from three independent experiments. (E) Pearson's coefficient between Exo70 and centrin-GFP at different times. *, $P = 0.0112$; ***, $P = 0.0009$; two-way ANOVA with Sidak's multiple comparison test; $n \geq 52$ cells from two independent experiments. Error bars are mean \pm SEM.

state (Meiri et al., 2012). Additionally, we observed that BCR engagement triggered the accumulation of GEF-H1 at the synaptic membrane as well as its association with Exo70 and Sec5, a known binding partner for GEF-H1 (Fig. 4, C and D, respectively). Thus, these results suggest that GEF-H1 could be involved in exocyst assembly during B cell activation. To this end, we silenced the expression of GEF-H1 in B cells by shRNA (Fig. S3 D) and evaluated the formation of exocyst complexes upon BCR stimulation. Our results show that GEF-H1-silenced B cells display unaltered recruitment of Exo70 toward the IS (Fig. S3 E) but fail to assemble the exocyst complex, normally observed

within 60 min of BCR stimulation (Fig. 4 E). Collectively, these results suggest GEF-H1 is activated and accumulates at the IS upon BCR engagement, promoting the assembly of the exocyst complex.

The stable recruitment of lysosomes at the IS relies on Exo70

Having shown how Exo70 is targeted to the IS upon BCR stimulation, we next investigated whether it played a role in the recruitment of lysosomes within this domain. For this purpose, we silenced the expression of Exo70 in the B cell line by shRNA (Fig. S4 A) and focused on the functional implications that the

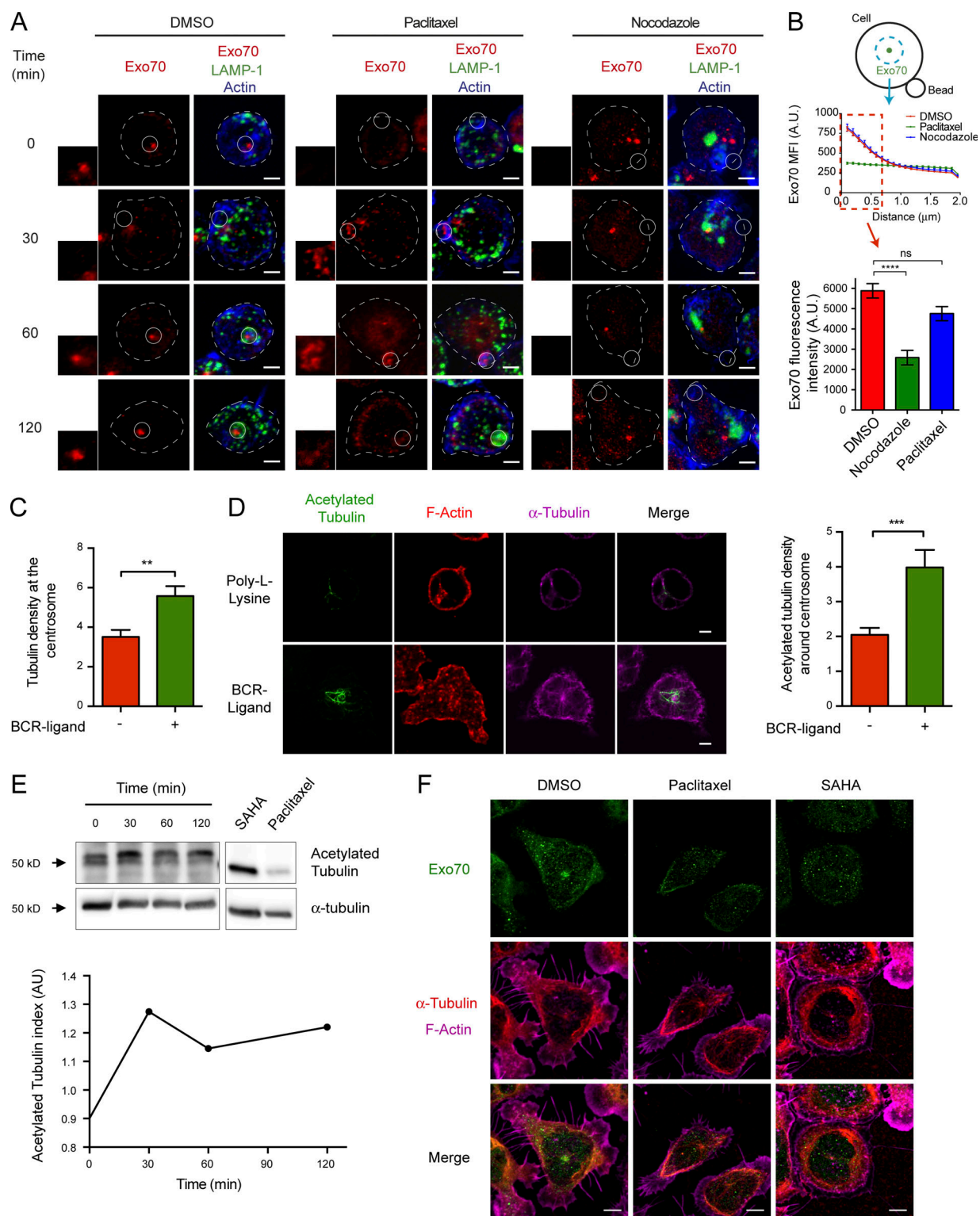


Figure 3. Localization of Exo70 at the centrosome is regulated by microtubule dynamics. (A) Z-projections of confocal images of B cells pretreated with DMSO, paclitaxel, or nocodazole for 1 h and activated with BCR ligand⁺ beads for the indicated times. Exo70 (red), LAMP-1 (green), and F-actin (blue). Insets highlight the IS area. Scale bar: 3 μ m. (B) Scheme depicting quantification of Exo70 MFI as a radial profile in a 3- μ m radius area from the brightest point of Exo70. Graph represents the MFI of Exo70 within the first 0.7 μ m of the graph, plotted for DMSO-, paclitaxel-, or nocodazole-treated cells. ****, $P < 0.0001$; two-way ANOVA with Sidak's multiple comparison test; $n \geq 80$ cells from two independent experiments. (C) Microtubule accumulation at the centrosome was quantified in resting or 60-min-activated B cells. $n \geq 31$ cells per time point from three independent experiments. **, $P = 0.0006$; unpaired t test; $n \geq 31$ cells from two independent experiments. (D) Left: B cells were seeded on poly-L-lysine or BCR-ligand⁺ coated coverslips for 60 min. Acetylated tubulin (green), α -tubulin (red), and F-actin (phalloidin, magenta). Scale bar: 3 μ m. Right: Quantification of the centrosomal acetylated tubulin. **, $P = 0.0032$; unpaired t test; $n \geq 49$ cells from two independent experiments. Error bars are mean \pm SEM. (E) B cells were activated as described in D. Top: Acetylated tubulin levels were

evaluated by Western blot. Bottom: Quantification of acetylated tubulin levels normalized by total tubulin levels. **(F)** Z-projections of confocal images of B cells seeded for 30 min on BCR ligand⁺ coated coverslips and then treated with paclitaxel 20 μ M or SAHA 1 μ M for 30 min. Exo70, green; α -tubulin, red; F-actin (phalloidin), magenta. Scale bar: 3 μ m.

deficiency of Exo70 could have on lysosome tethering and fusion at the synaptic membrane. Lower levels of the LAMP-1 marker were observed in synaptic membranes isolated from Exo70-silenced B cells compared with controls, suggesting that Exo70 is required for the fusion of lysosomes at the IS (Fig. 5 A). To evaluate this phenotype further, we performed image analysis in

which B cells were activated with BCR ligand⁺ beads and stained for CEP55 and LAMP-1 to label the centrosome and lysosomes, respectively (Fig. 5 B). Calculated centrosome and lysosome polarity indexes (Fig. S4 B) indicated that Exo70-silenced cells did not present defects in repositioning of the centrosome toward the IS (Fig. 5 C). However, polarized lysosome recruitment

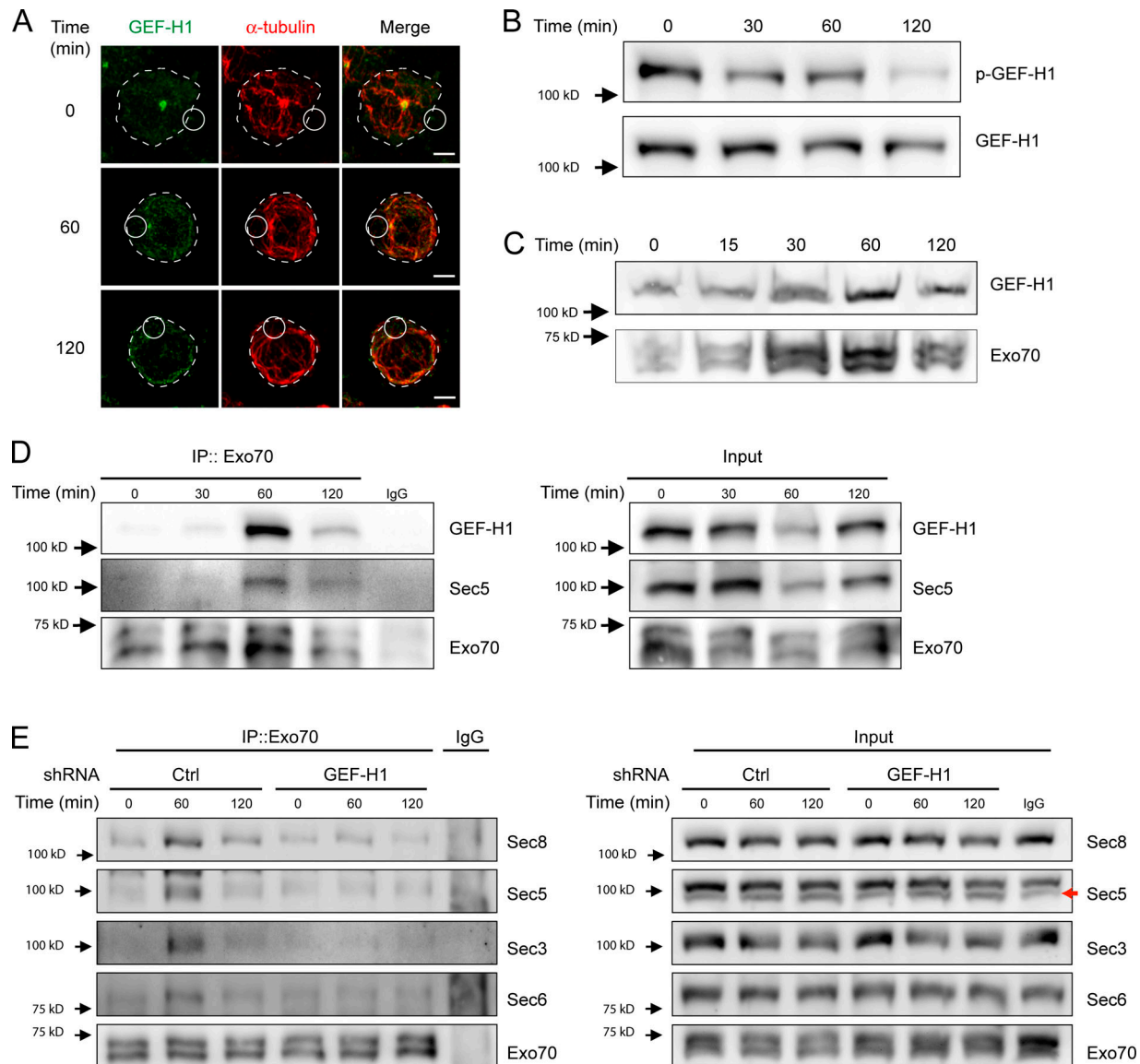


Figure 4. GEF-H1 accumulates at the IS of B cells and is required for exocyst assembly. **(A)** Representative confocal images of B cells activated with BCR ligand⁺ coated beads for different times. GEF-H1 (green) and α -tubulin (red). Scale bar: 3 μ m. **(B)** B cells were activated on BCR ligand⁺ coated plates for different times, and p-GEF-H1 and total GEF-H1 were detected by Western blot. Representative of three independent experiments. **(C)** Detection of GEF-H1 in synaptic membranes. B cells were stimulated with BCR ligand⁺ Dynabeads for the indicated times, and GEF-H1 was detected in isolated synaptic membranes by Western blot. Representative of two independent experiments. **(D)** B cells were activated as described in B, and Exo70 was immunoprecipitated (IP) from corresponding lysates. Associated GEF-H1 and Sec5 were detected by Western blot. Representative of four independent experiments. **(E)** Control or GEF-H1-silenced B cells were activated as in B, and the formation of exocyst complexes was evaluated by immunoprecipitating Exo70 from lysates. Sec8, Sec5, Sec3, Sec6, and Exo70 were detected by Western blot. Red arrow specifies the band corresponding to Sec5. Representative of two independent experiments.

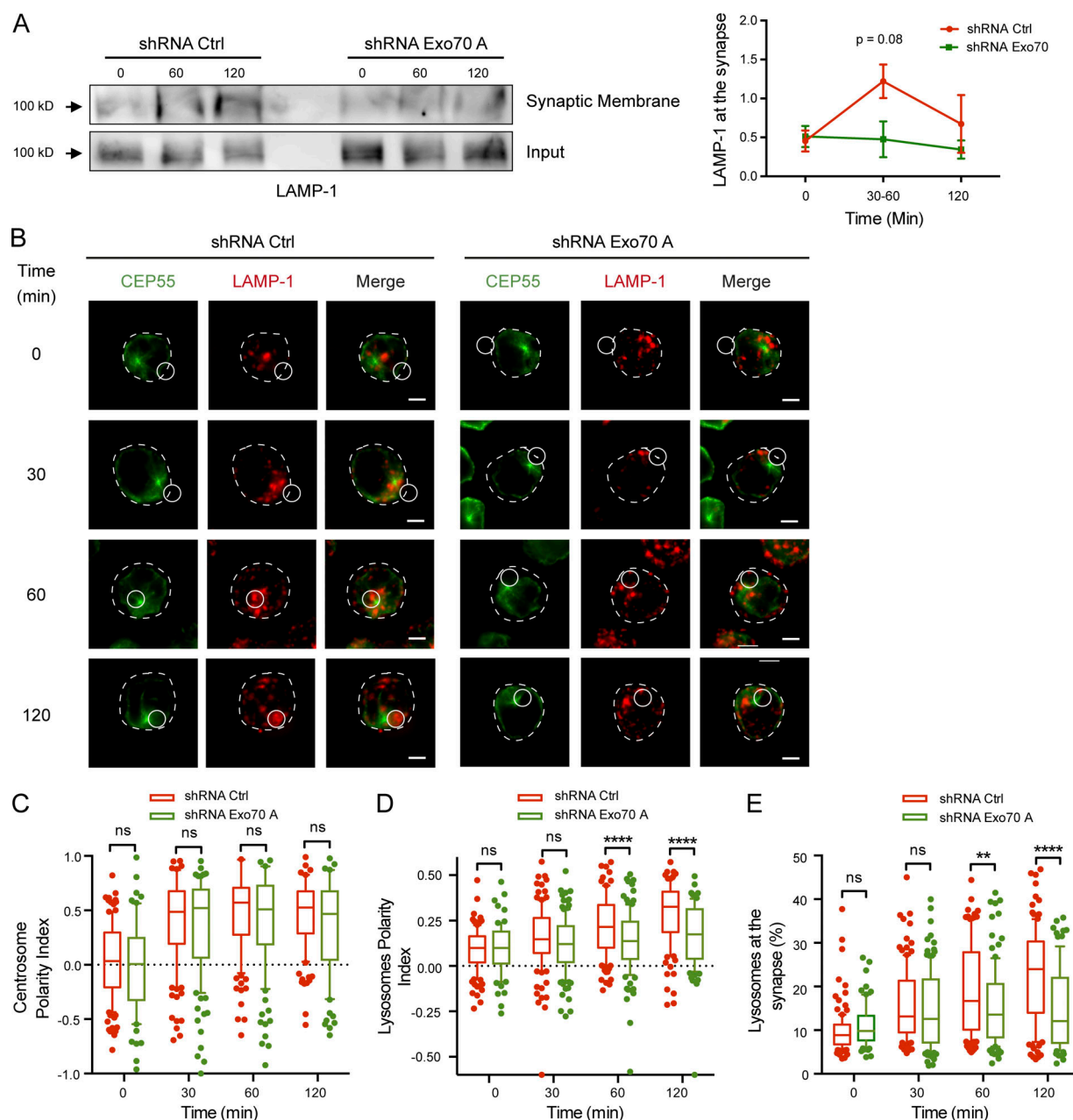


Figure 5. Exo70-silenced B cells display deficient lysosome stabilization and fusion at the IS. (A) Control or Exo70-deficient B cells were stimulated with BCR ligand⁺ Dynabeads for indicated times, and synaptic membranes were isolated. Left: Detection of LAMP-1 by Western blot. Right: Quantification of LAMP-1 normalized to input protein levels in total lysates from four independent experiments. Error bars are mean \pm SEM. (B) Representative images of B cells stained for the centrosome (CEP55, green) and lysosomes (LAMP-1, red) after indicated activation times with BCR ligand⁺ beads. The centrosome plane of the CEP55 staining is shown along the Z-projection of LAMP-1. Scale bar: 3 μ m. (C–E) Quantification of centrosome and lysosome polarity indexes (C and D) and lysosome accumulation (E) at the IS. **, $P = 0.0026$; ****, $P < 0.0001$; ANOVA with Sidak's multiple comparison test. $n \geq 70$ cells from two independent experiments. ns, not significant.

to the IS was impaired in Exo70-silenced cells (Fig. 5 D), which was particularly evident at later time points where lysosomes stably accumulated at the antigen-bead contact site in control cells but to a lesser extent in Exo70-silenced cells. Accordingly, the percentage of lysosomes that accumulated around the BCR ligand⁺ bead was significantly lower (Figs. 5 E and S4 C). Thus, we conclude that Exo70 is required for the stable recruitment of lysosomes at the IS of B cells.

Exo70 regulates lysosome tethering and secretion at the IS of B cells

We next evaluated whether Exo70 was directly involved in tethering lysosomes at the IS. For this purpose, we imaged the cell juxtamembrane region of B cells in contact with immobilized antigen by confocal microscopy. Control and Exo70-silenced B cells were seeded onto antigen-coated slides for 60 min, fixed, and labeled with LAMP-1 to analyze the

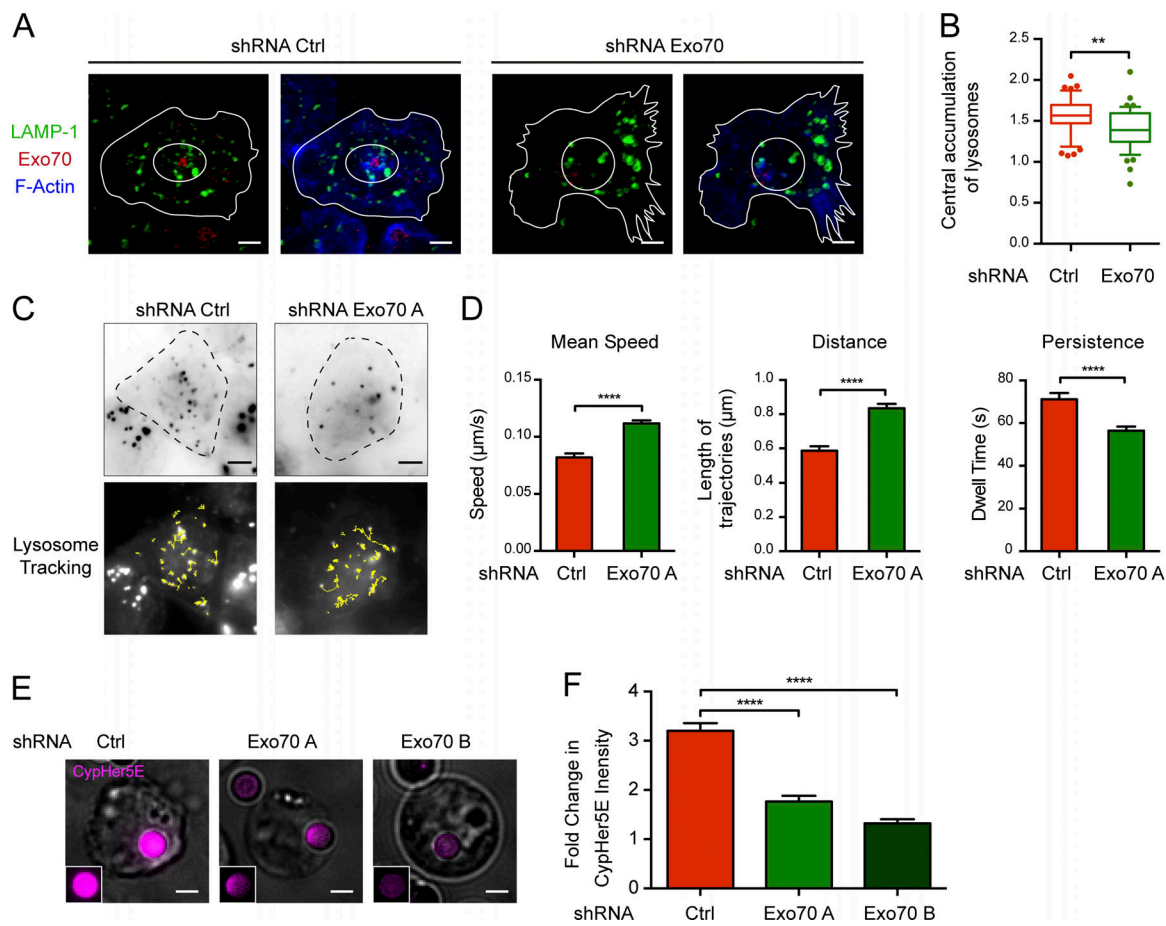


Figure 6. Defective lysosome docking and secretion at the IS of Exo70-silenced cells. (A) Confocal images of control and Exo70-silenced cells activated on BCR ligand⁺ coverslips for 60 min. LAMP-1 (green), Exo70 (red), and F-actin (blue). Scale bar: 3 μm. (B) Ratio between the central and peripheral lysosomes in the cell. **, $P = 0.001$; unpaired t test; $n \geq 44$ cells from two independent experiments. (C) Top: TIRF images of LysoSensor Green-stained lysosomes at IS of control and Exo70-silenced B cells plated on BCR ligand⁺ coated slides. Bottom: Lysosome trajectories of the TIRF images are shown as yellow lines. Scale bar: 5 μm. (D) Quantification of dynamic parameters of lysosomes at the IS. ****, $P < 0.0001$; unpaired t test; $n \geq 500$ lysosome trajectories from ≥ 14 cells per condition from two independent experiments. Error bars are mean \pm SEM. (E) Representative epifluorescence images of Exo70-silenced or control cells activated with CypHer5E-coupled BCR ligand⁺ beads for 90 min. Cells are shown as Z-projections of a stack. Insets highlight the CypHer5E fluorescence in the bead. Scale bar: 3 μm. (F) Quantification of the bead CypHer5E intensity, normalized by the intensity of noninteracting beads. ****, $P < 0.0001$; two-way ANOVA with Sidak's multiple comparison test; $n \geq 160$ cells from two independent experiments. Error bars are mean \pm SEM.

distribution of lysosomes at this interface (Fig. 6 A). Activated B cells present a radial distribution of lysosomes at the synaptic membrane, where they are highly concentrated at the center of the synapse, previously described as the secretory domain in NK and cytotoxic T cells (Stinchcombe et al., 2001). In contrast, Exo70-silenced B cells displayed disorganized lysosomes that did not coalesce at the center of the IS (Fig. 6 B), suggesting that lysosome dynamics was altered in these cells. To confirm this observation, we used total internal reflection fluorescence (TIRF) microscopy to track lysosome dynamics in control and Exo70-silenced cells attached to antigen-coated dishes. 3-min-long movies were acquired, and lysosomes labeled with LysoSensor Green were followed in the evanescent field (Fig. 6 C and Video 1). Interestingly, lysosomes from Exo70-deficient cells present highly dynamic behavior compared with control cells, displaying a faster mean velocity, longer trajectories, and lower dwelling times at the synaptic membrane (Fig. 6 D), suggesting that they were unable to stably attach to the synaptic membrane.

Thus, our findings strongly suggest that Exo70 is required to promote the tethering of lysosomes at the IS upon activation of B cells with immobilized antigen. Given that tethering is a prerequisite for docking and fusion of secretory vesicles, we decided to directly assess the role of Exo70 on lysosome secretion at the IS. Control and Exo70-silenced cells were incubated with beads containing BCR ligand⁺ coupled to CypHer5E, a dye whose fluorescence increases at acidic pH (Milasta et al., 2005). This method has been previously used to measure local pH acidification at the IS in B cells, which correlates with local exocytosis of lysosomes (Yuseff et al., 2011). Consistent with the above results, we observed that Exo70-silenced cells displayed a decrease in fluorescent signals at the interface between B cells and CypHer5E-coated activating beads, indicating a defect in lysosome secretion at this level (Fig. 6, E and F). Altogether, our data suggest that Exo70 promotes the tethering of secretory lysosomes at the synaptic membrane, which is critical for their fusion at the IS.

The exocyst is required for the extraction and presentation of immobilized antigens by B cells

Silencing the expression of proteins that regulate polarized lysosome secretion at the IS of B cells dramatically affects their capacity to extract and present immobilized antigens in vitro (Yuseff et al., 2011; Reversat et al., 2015). We therefore investigated whether analogous defects were observed in Exo70-silenced cells. For this, antigen extraction was first evaluated by measuring the fluorescence signal of ovalbumin (OVA) remaining on activating (BCR ligand⁺) beads after their interaction with control or Exo70-silenced cells. Indeed, higher levels of OVA were detected on beads interacting with Exo70-silenced B cells in comparison to control cells (Fig. 7 A), suggesting that antigen extraction was impaired. Importantly, no major differences in BCR surface levels were observed between control and Exo70-silenced cells (Fig. S4 D), suggesting that defects in antigen extraction did not result from impaired activation or interaction with antigens. We then tested whether the decreased capacity of Exo70-silenced cells to efficiently extract immobilized antigens also had an impact on their ability to present such antigens. For this, we incubated control and Exo70-silenced cells with beads coupled to a specific BCR ligand together with the *Lack* antigen from *Leishmania major*. The ability of the cells to present MHC-II-peptide complexes derived from bead-associated *Lack* to a specific T cell hybridoma was then measured by monitoring IL-2 secretion by activated T lymphocytes. As expected, presentation of bead-associated *Lack* antigen to T lymphocytes was strongly impaired in Exo70-silenced cells (Fig. 7 B). Importantly, no defects were observed in the presentation of the *Lack* peptide by these cells, indicating that silencing of Exo70 does not have an impact on B-T cell interactions. Noticeably, silencing Sec3 and Sec8 also led to impaired antigen extraction and presentation (Fig. S5), suggesting that Exo70 probably acts in concert with other exocyst components to regulate the extraction and presentation of immobilized antigens. Finally, considering that GEF-H1 is critical for exocyst assembly during B cell activation, we evaluated whether GEF-H1-silenced cells also had defects in antigen extraction and presentation. Indeed, our results show that GEF-H1-deficient cells are unable to efficiently extract and present immobilized antigen (Fig. 7, C and D), which most likely results from impaired lysosome fusion as evidenced by the lack of LAMP-1⁺ rings in activated B cells silenced for GEF-H1 (Fig. 7 E). Collectively, these data reveal how exocyst-dependent tethering and fusion of lysosomes at the IS play critical roles in regulating immune effector functions of B cells at the IS.

Discussion

The molecular mechanisms that orchestrate the delivery and secretion of lysosomes within precise domains of the plasma membrane remain largely unknown. We provide insight to this process by revealing that BCR engagement (a) enhances microtubule acetylation, releasing Exo70 from the centrosome to allow its recruitment to the IS, and (b) activates GEF-H1, which promotes the assembly of the exocyst complex,

thereby regulating the local recruitment and secretion of lysosomes at the synaptic membrane (Fig. 8).

Assembly of the exocyst in B cells is very dynamic and peaks upon 60 min of activation, which correlates with our imaging analysis showing that lysosomes are stably docked at this time. After longer times of activation (120 min), we observed the formation of a LAMP-1⁺ ring, suggesting that fusion has taken place and the exocyst is probably no longer required. Considering the timeline of events leading up to lysosome fusion, we suggest that Exo70 assembly promotes lysosome tethering and might quickly disassemble. We propose that this could be required to recycle exocyst subunits required to extract other antigens in subsequent synapses formed by B cells.

In resting B cells, Exo70 mainly accumulates at the centrosome, while Sec3 is partially associated with lysosomes. However, both subunits reach the synaptic membrane upon activation and become assembled into a complex upon BCR engagement. Although we do not know exactly where the exocyst complex is being assembled, it is possible that exocyst assembly could take place at the synaptic membrane or within the membrane of lysosomes recruited at the IS, as reported in a yeast model (Bendezú et al., 2012). Additionally, we cannot rule out that exocyst subcomplexes are being formed upon BCR engagement; however, recent studies support the idea that the exocyst functions as a stable holocomplex (Heider et al., 2016), which coincides with our results, as we did not detect subcomplexes associated with Exo70.

In agreement with our findings, reports on NK cells have shown that Ral-GTPases A and B, known effectors of the exocyst, promote granule secretion at the IS and thereby regulate NK cytotoxicity (Sánchez-Ruiz et al., 2011). While B cells do not undergo classic granule secretion to promote the killing of target cells, as NK or cytotoxic T cells do (Stinchcombe et al., 2006; Jenkins et al., 2009), they secrete lysosomes at the synaptic interface to facilitate the extraction of antigens, particularly those presented on rigid substrates (Natkanski et al., 2013). By mediating the initial contact between secretory vesicles and the plasma membrane, the exocyst also has an impact on SNARE assembly, which is required for vesicle fusion (He and Guo, 2009; Heider and Munson, 2012; Wu and Guo, 2015). This is highlighted by the fact that Sec3 and Sec6, part of the exocyst complex, are able to modulate SNARE assembly at the membrane of yeast (Morgera et al., 2012; Shen et al., 2013; Yue et al., 2017). In B cells, defective lysosome secretion generated by silencing the SNARE protein Vamp7 also impairs the extraction and presentation of immobilized antigens (Obino et al., 2017). Whether Exo70 and/or other subunits of the exocyst complex interact with Vamp-7 to promote the docking of Vamp-7⁺ vesicles at the IS shall be further explored.

B cells display a large pool of Exo70 tightly associated to the centrosome, which is sensitive to microtubule dynamics. Stabilization of microtubules surrounding the centrosome is enhanced upon BCR engagement, which acts as a signal to deplete Exo70 from the centrosome, thereby promoting its accumulation at the synaptic membrane. Intriguingly, while microtubule density at the centrosome is increased by B cell activation, actin has been reported to decrease at this level (Obino et al., 2016).

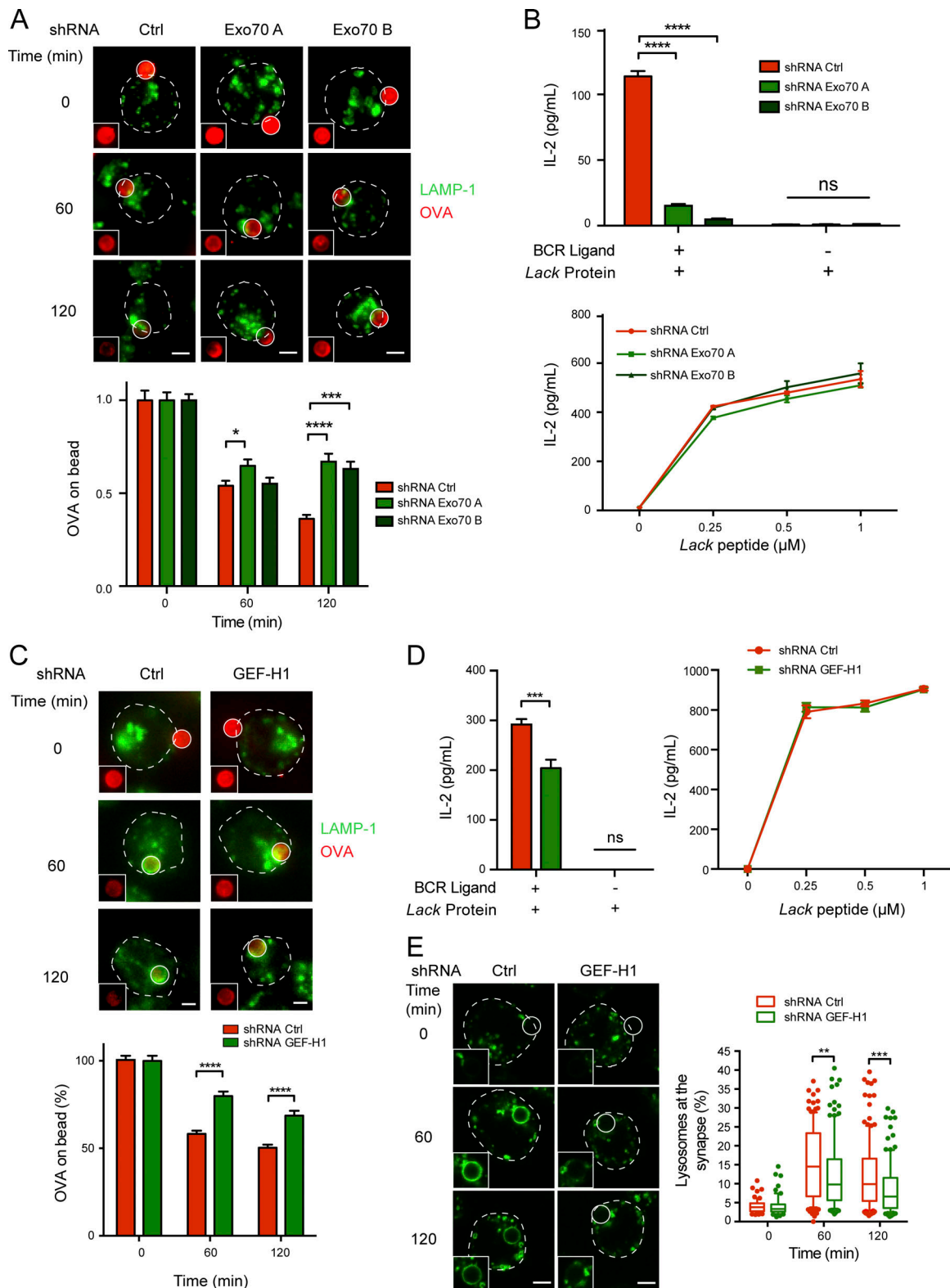


Figure 7. Impaired antigen extraction and presentation in Exo70-silenced and GEF-H1 silenced cells. (A and C) Antigen extraction assay. Top: Representative epifluorescence images of control and Exo70-silenced (A) or GEF-H1-silenced (C) cells incubated with BCR ligand⁺ beads coupled to OVA for the indicated times. Cells were fixed and stained for OVA (red) and LAMP-1 (green). Images are shown as Z-projections of a stack. Insets highlight the remaining OVA fluorescence intensity on the bead. Scale bar: 3 μ m. Bottom: Quantification of OVA fluorescence intensity remaining on beads. Values were normalized by the initial fluorescence. *, $P < 0.05$; ***, $P < 0.001$; ****, $P < 0.0001$; two-way ANOVA with Sidak's multiple comparison test; Exo70: $n \geq 59$ cells from two independent experiments; GEF-H1: $n \geq 73$ cells from three independent experiments. **(B and D)** Antigen presentation assays. Top: Antigen presentation assay with control and Exo70-silenced (B) or GEF-H1-silenced (D) cells. Bottom: Peptide control for the cells used. Mean amounts of IL-2 are shown for a

representative of three independent experiments performed in triplicate for Exo70-silenced cells, two independent experiments for GEF-H1-silenced cells. ***, $P = 0.0006$; ****, $P < 0.0001$; two-way ANOVA with Sidak's multiple comparison test. Error bars are mean \pm SEM. (E) Representative images of lysosome recruitment to antigen-coated beads in control and GEF-H1-silenced cells. **, $P < 0.01$; ***, $P < 0.001$; two-way ANOVA with Sidak's multiple comparison test; $n \geq 93$ cells from three independent experiments.

Actin depletion allows the detachment of the centrosome from the nucleus and thereby promotes its polarization to the IS; however, actin-depolymerizing drugs did not affect the centrosome-associated pool of Exo70. This result was unexpected, considering that Exo70 has been tightly associated with actin and can directly interact with the Arp2/3 complex to promote actin branching independently of the other exocyst subunits (Liu et al., 2012). However, considering that the Arp2/3 complex is also recruited to the IS upon B cell activation, we cannot exclude that interactions between Arp2/3 and Exo70 might coordinate actin cytoskeleton remodeling at the synaptic membrane, analogously to what occurs during lamellipodia formation at the leading edge of migrating fibroblasts (Liu et al., 2012). Whether potential actin rearrangements promoted by Exo70 at the IS are coupled to Myosin II activity to generate pulsing forces that contribute to antigen extraction should be explored. Exo70 has also been reported to interact with microtubules and can inhibit microtubule polymerization in vitro (Wang et al., 2004). Thus, it is tempting to speculate that the subcellular localization of Exo70 can balance the interplay between microtubule and actin cytoskeletons, inhibiting the polymerization of microtubules to favor actin enrichment at the centrosome. Stabilization of the microtubule network near the centrosome triggered by B cell activation is promoted by increased acetylation. This posttranslational modification can regulate microtubule-dependent trafficking in diverse cells types by controlling centrosome repositioning or restricting kinesin-dependent vesicle movements (Bhuwanya et al., 2014; Dubois et al., 2017). Thus, acetylation of microtubules triggered upon B cell activation could coordinate the accumulation of lysosomes at the centrosome with Exo70-dependent lysosome fusion at the synaptic membrane, thereby enabling the

spatial-temporal control of lysosome fusion within a defined region of the plasma membrane.

How are changes in microtubule dynamics coupled to the assembly of the exocyst complex in B cells? We show that the rho activating factor GEF-H1, which is associated with the microtubule network and is required for exocyst assembly in other cell types (Pathak et al., 2012), accumulates at the IS and promotes the assembly of the exocyst complex upon B cell activation. Interestingly, GEF-H1 has been described as a regulator of immune effector functions. In neutrophils, GEF-H1 enables shear stress-induced transendothelial cell migration to inflamed tissues (Fine et al., 2016), and in macrophages, recognition of nucleic acids by RIG-I-like receptors triggers GEF-H1 dissociation from microtubules to enhance antiviral responses (Chiang et al., 2014). Intriguingly, higher extracellular matrix stiffness leads to the activation of GEF-H1 in epithelial cells (Heck et al., 2012). Thus, the rigid nature of the substrate in which antigens are presented in our assay might act as a costimulatory signal to release GEF-H1 from microtubules and promote exocyst-dependent proteolytic antigen extraction instead of force-mediated antigen extraction. In contrast to epithelial cells, where activation of GEF-H1 is dependent on microtubule depolymerization, our data show that its activation is coupled to the stabilization of microtubules (Birukova et al., 2010; Heck et al., 2012). Additionally, BCR downstream signaling could enhance GEF-H1 activation, given that phosphorylation dependent on extracellular signal-regulated kinases in Thr678 promotes its guanine nucleotide exchange activity (Jacob et al., 2002; Fujishiro et al., 2008; Kakiashvili et al., 2009).

How does Exo70 interact with the synaptic membrane? In yeast and mammalian epithelial cells, both Sec3 and Exo70 bind

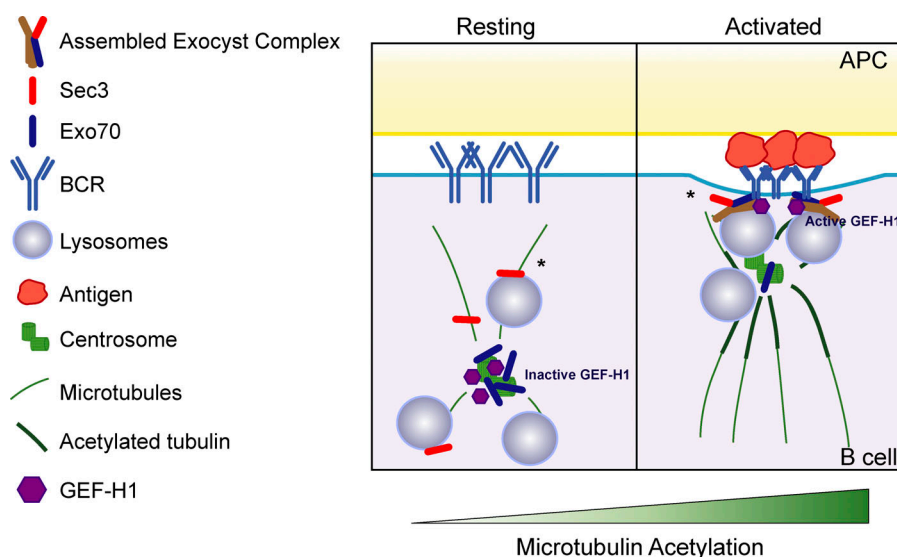


Figure 8. Scheme depicting how the recruitment of the exocyst at the IS is regulated. In resting conditions, Exo70 is mainly associated to the centrosome and inactive GEF-H1 to microtubules. BCR engagement enhances microtubule acetylation surrounding the centrosome, which releases Exo70 allowing its recruitment to the IS, and activates GEF-H1, which promotes the assembly of the exocyst complex to support local lysosome fusion at the synaptic membrane. Asterisk indicates that the localization of Sec3 and the site of exocyst assembly remain to be elucidated. APC, antigen-presenting cell.

to the plasma membrane by interactions with the phospholipid phosphatidylinositol 4,5-bisphosphate (He et al., 2007; Liu et al., 2007; Zhang et al., 2008; Baek et al., 2010). This interaction relies on a patch of basic residues at the carboxyl and amino termini of Exo70 and Sec3, respectively (Dong et al., 2005; Hamburger et al., 2006; He et al., 2007; Liu et al., 2007; Moore et al., 2007). Although we cannot rule out that direct binding to phospholipids enriched at the synaptic membrane may contribute to the stable attachment of Exo70 within IS, spatial and temporal control of exocyst-mediated secretion also relies on polarity complexes and rho GTPases. For instance, in COS1 cells, Cdc42 directly interacts with Exo70, promoting the exocyst complex assembly required for phagosome formation (Mohammadi and Isberg, 2013), and is an essential regulator of B cell polarity (Yuseff et al., 2011). Furthermore, recent observations made in epithelial cells showed that Exo70 can bind directly to the polarity complex protein Par3 at cellular junctions of the plasma membrane, a process that supports local membrane delivery and epithelial cell survival (Ahmed and Macara, 2017). Accordingly, lysosomes are not efficiently docked at the IS of Par3-silenced cells (Reversat et al., 2015), which could be explained by the failure of these cells to recruit Exo70 to the synaptic membrane. In agreement with these results, TC10, a GTPase known to target Exo70 to the plasma membrane (Pommereit and Wouters, 2007; Dupraz et al., 2009; Fujita et al., 2013), was recently shown to be required for B cell responses in vivo: TC10 knockout mice show defects in IgM responses and germinal cell formation (Burbage et al., 2017). Thus, polarized targeting of the exocyst complex by the concerted action of polarity proteins and GTPases emerges as a key mechanism to regulate B cell activation.

Overall, our work reveals that Exo70 acts as a landmark for lysosome secretion at the IS and is therefore critical to promote the extraction and presentation of immobilized antigens. We propose that the centrosome of B cells acts as a hub that focuses specialized cellular machinery, which is mobilized to the IS upon antigen engagement and is used to regulate membrane trafficking at this level. Our results bring forward novel mechanistic insight on how BCR engagement triggers changes in microtubule dynamics to orchestrate the recruitment of effector molecules at the IS. We predict that Exo70 and/or other components of the exocyst complex could also modulate key trafficking events required for target cell killing or cytokine secretion in other cells of the immune system.

Materials and methods

Mice, cells, and cell culture

The mouse IgG⁺ B-lymphoma cell line IIA1.6 (Jones et al., 1986; Lankar et al., 2002) and the LMR7.5 T cell hybridoma that recognizes I-A^d-Lack_{156–173} complexes (Malherbe et al., 2000; Le Roux et al., 2007; Vascotto et al., 2007) were obtained from A.-M. Lennon-Duménil. The cells were cultured in CLICK medium (RPMI 1640 with Glutamax supplemented with 10% heat-inactivated FBS, 0.1% 2-mercaptoethanol, 100 U/ml penicillin, 100 µg/ml streptomycin, and 1 mM sodium pyruvate). HEK 293T cells were cultured for lentiviral production in DMEM supplemented with 10% FBS and penicillin/streptomycin. All cell

culture products were purchased from Life Technologies. Spleen B cells were isolated from C57BL/6 mice using a magnetic-activated cell sorting B cell isolation kit (Miltenyi) according to the manufacturer's instructions. All animal work was reviewed and approved by the Institutional Scientific Ethics Committees for Animal and Environmental Care and Research Biosafety, Pontificia Universidad Católica de Chile (protocol number 170709007).

Antibodies

The following primary antibodies were used for immunofluorescence: rat anti-LAMP-1 (BD Biosciences; #553792, 1:200), rabbit anti-CEP55 (Abcam; #ab170414, 1:500), rabbit anti-Exo70 (Abcam; #ab95981, 1:200), rabbit anti-HA (Abcam; #ab137838, 1:500); rabbit anti-GEF-H1 (Abcam; #ab155785, 1:200), rat anti- α -tubulin (Abcam; #ab6160, 1:500), rabbit anti-acetyl- α -tubulin (Lys40; Cell Signaling; #5335, 1:200), rabbit anti-OVA (Sigma-Aldrich; #C6534, 1:500), and Alexa Fluor 546-conjugated goat anti-mouse IgG (Thermo Fisher Scientific; #A11018, 1:200). The following secondary antibodies were used: Alexa Fluor 488-, Alexa Fluor 568-, Cy3-, and Alexa Fluor 647-conjugated F(ab')₂ donkey anti-rat and Cy3-conjugated F(ab')₂ donkey anti-rabbit (Jackson ImmunoResearch; 1:200); and Alexa Fluor 488-conjugated goat anti-rabbit (Thermo Fisher Scientific; 1:200). F-actin was stained using Alexa Fluor 546- or Alexa Fluor 647-conjugated phalloidin (Life Technologies; #A22283 and #A22287, respectively, 1:200). For Western blot, the following antibodies were used: rabbit anti- γ -tubulin (Abcam; #Ab11317, 1:1,000); mouse anti-actin (clone C4, ImmunO; #691001); rabbit anti-pGEF-H1 (Ser885; clone E1L6D, Cell Signaling; #14143); rabbit anti-LAMP-1 (Cell Signaling; #C54H11, 1:1,000), rabbit anti-Sec3 (Proteintech; #11690-1-AP, 1:1,000), mouse anti-Exo70, anti-Sec5, anti-Sec6, and anti-Sec8 antibodies (clone 13F3, 1.1, 9H5, and 8F12, respectively), provided by C. Yeaman. As secondary antibody, HRP-conjugated donkey anti-mouse, anti-rat, or anti-rabbit (Jackson ImmunoResearch; 1:5,000) was used. For immunoprecipitation, we used the mouse anti-Exo70 mAb (clone 13F3, 1:200).

Plasmids

The eGFP-Centrin1 plasmid was obtained from M. Bornens (Institut Curie, Paris, France). The Sec3-HA plasmid was kindly provided by P. Chavrier (Institut Curie, Paris, France). Plasmid expression was achieved by electroporating 2×10^6 B-lymphoma cells with 2 µg of plasmid using the Amaxa Cell Line Nucleofactor Kit R (L-013 program; Lonza). Cells were incubated in CLICK medium for 16–20 h before analysis.

Lentiviral production and infection

The shRNAs used to silence the IIA1.6 B cells were purified from Mission shRNA Bacterial Glycerol Stocks (Sigma-Aldrich): shRNA Exo70 A TRCN0000366721, shRNA Exo70 B TRCN0000366722, shRNA Sec3 A TRCN0000127656, shRNA Sec8 A TRCN0000298307, and control shRNA SHC016. GEF-H1 shRNA bacterial glycerol stock was purchased from Open Biosystems (Dharmacon): TRCN0000109985. Lentiviruses were produced by transfection in a 1:2.5:3 ratio of the envelope (pVsVG), the packaging (pPAX-2), and shRNA-encoding

plasmids in 293T cells with FuGene HD Transfection Reagent (Promega). Silencing efficiency was confirmed by Western blot as described below. IIA1.6 cells were infected by 24-h incubation with viral supernatants. After 48 h, puromycin selection (5 μ g/ml) was performed, and cells were assayed 72 h later.

Reagents and drugs

The *Lack* antigen was produced and purified from bacteria through histidine tag purification with Ni-NTA agarose beads (Invitrogen), and the *Lack* peptide (aa 156–173) was synthesized by PolyPeptide Group. CypHer5E was purchased from Amersham Bioscience and used according to the manufacturer's instructions. For cytoskeleton-disrupting drugs, we used 10 μ M nocodazole, 5 μ M Latrunculin A, and 20 μ M paclitaxel (Merck). For histone deacetylase inhibition, we used 1 μ M SAHA (Cayman Chemical Company).

Preparation of BCR ligand-coated beads

4×10^7 3- μ m latex NH₂ beads (Polyscience) were activated with 8% glutaraldehyde (Sigma-Aldrich) for 4 h at room temperature (Batista and Neuberger, 2000; Yuseff et al., 2011; Yuseff and Lennon-Dumenil, 2013). Beads were washed with PBS and incubated overnight at 4°C with different ligands: 100 μ g/ml of either F(ab')₂ goat anti-mouse IgG (BCR ligand⁺ beads) or F(ab')₂ goat anti-mouse IgM (BCR ligand⁻ beads; MP Biomedical) in combination or not with 100 μ g/ml of the *L. major* antigen *Lack* or 100 μ g/ml of OVA.

B cell stimulation and immunofluorescence

Cells were plated on poly-L-lysine-coated slides and stimulated with indicated beads at a 1:1 ratio (cell/beads) for indicated times at 37°C and fixed in 4% paraformaldehyde for 10 min at room temperature. For acetylated tubulin staining, cells were fixed with microtubule buffer (60 mM Pipes, 25 mM Hepes, 5 mM EGTA, 1 mM MgCl₂, 0.1% Triton X-100, and 0.5% glutaraldehyde, pH 7) for 15 min on ice. Fixed cells were incubated for 60 min with primary antibodies and 60 min with secondary antibodies in PBS-BSA-saponin (1 \times /0.2%/0.05%). Coverslips were mounted on slides using Fluoromount G (Electron Microscopy Sciences).

Immunofluorescence image acquisition and analysis

Epifluorescence microscopy images were acquired using a 63 \times /1.4-NA oil-immersion objective on an Eclipse Ti microscope (Nikon Instruments) equipped with a iXon Ultra EMCCD camera (Andor) and operated by NIS-Elements Advanced Research imaging software. Confocal images were acquired using an inverted microscope FV1000 (Olympus) with a 60 \times /1.35-NA objective or an inverted spinning disk confocal microscope (Roper/Nikon) with a 60 \times /1.4-NA oil-immersion objective. Image processing was performed with Fiji (ImageJ; National Institutes of Health) software. Single-cell images shown in the figures were cropped from large fields, and their contrast and brightness were manually adjusted using ImageJ.

Polarity analysis

Centrosome, Exo70, and LAMP-1 polarity indexes were calculated as described previously (Reversat et al., 2015). Briefly,

using the macro, we manually selected the bead and the cell area from which the cell and bead center were extracted (Bead_C and Cell_C, respectively). Then z-stacks were projected from which, for discrete staining (Centrosome and Exo70), we manually selected a coordinate representing the localization, and for the lysosomes, the center of mass of the LAMP-1 staining was obtained (Label_C). The distance between Label_C and Cell_C was projected on the Bead_C–Cell_C axis by multiplying by the cosine of the angle described by Label_C–Cell_C–Bead_C. The polarity index was calculated by dividing the projected Cell_C–Label_C distance by the Cell_C–Bead_C distance. The index ranges from –1 (anti-polarized) to 1 (fully polarized).

Lysosome recruitment

Accumulation of lysosomes at the IS was quantified by measuring the LAMP-1 fluorescence intensity in a concentric circular area closely surrounding the bead (3.5 μ m) and normalized by the whole cell LAMP-1 fluorescence intensity. The radial distribution of lysosomes was calculated by measuring the LAMP-1 mean fluorescence intensity (MFI) in concentric rings of 2% increasing steps starting from the bead and normalized by the whole cell LAMP-1 MFI.

Local accumulation of Exo70, α -tubulin, or acetylated tubulin

First, a circle with a 3- μ m radius was drawn around the area of interest (the centrosome or the brightest Exo70 MFI). Next, the area delimited by the fluorescence intensity decrease <70% fluorescence of Exo70 (0.7 μ m), α -tubulin (0.5 μ m), and acetylated tubulin (0.5 μ m) was determined in a radial distribution profile, starting from the center of the circular area on resting cells (Obino et al., 2016) and was used to quantify MFIs of different labels in activating conditions or in the presence of drugs used to perturb the cytoskeleton. The MFI for Exo70, α -tubulin, or acetylated tubulin obtained in the z-projection of the three planes above and below the intensity peak was compared with the MFI of the whole cell. Because methanol fixation required for γ -tubulin was not compatible with the Exo70 staining, the centrosome was stained with antibodies directed against α -tubulin, and images were processed (fluorescence intensity threshold) to visualize the centrosome, as described previously (Obino et al., 2016).

TIRF microscopy

TIRF microscopy was performed on a Nikon Eclipse Ti inverted microscope equipped with a 100 \times /1.49-NA oil-immersion objective and a Quantem512SC Roper electron-multiplying CCD camera at 37°C/4.5% CO₂. Exo70-silenced or control B cells were stained with LysoSensor Green DND-189 (Life Technologies; #L7535) and attached on BCR ligand⁺-coated 35-mm dishes (Fluorodish) at 37°C. After 30 min, images were acquired with MetaMorph software and analyzed using ImageJ. The Track-Mate v2.8.1 plug-in from Fiji (Schindelin et al., 2012) was used to follow trajectories from LysoSensor Green-stained lysosomes.

Antigen-extraction assay

OVA and BCR ligand were coupled to beads in equal concentrations. Cells incubated in a 1:1 ratio with antigen-coated beads

were plated on poly-L-lysine slides for different times at 37°C, fixed, and stained for OVA. The amount of OVA present on the beads was calculated by measuring the fluorescence intensity of a fixed area around beads in contact with cells from a 3D projection of a z-stack (Fiji).

Antigen presentation

B cells were incubated with *Lack* ± BCR ligand⁺ beads or pre-processed peptide for 2–3 h. Cells were washed with PBS, fixed in ice-cold PBS/0.01% glutaraldehyde for 1 min, and quenched with PBS/100 mM glycine. B cells were then incubated with *Lack*-specific T cell hybridoma in a 1:1 ratio for 4 h (Yuseff et al., 2011; Yuseff and Lennon-Dumenil, 2013). Supernatants were collected, and IL-2 cytokine production was assessed with the BD optEIA Mouse IL-2 ELISA set following the manufacturer's instructions (BD Biosciences).

Centrosome purification

After stimulation with BCR ligand⁺ beads for 60 min, cells were incubated on ice with 200 nM nocodazole and 1 µg/ml cytochalasin D for 60 min. Cells were washed with TBS (10 mM Tris-HCl and 150 mM NaCl, pH 7.4) and resuspended on TBS 0.1× + 0.8% sucrose. The cells were lysed by adding 1:3 lysis buffer (1 mM Hepes, 0.5% NP-40, 0.5 mM MgCl₂, and 0.1% 2-mercaptoethanol, pH 7.2). The lysate was centrifuged at 10,000 rpm for 10 min at 4°C, and the supernatant was recovered. Centrosomes were isolated by sequential centrifugations at (a) 10,000 g for 30 min at 4°C on top of a 60% wt/vol sucrose cushion (10 mM Pipes, 0.1% Triton X-100, 0.1% 2-mercaptoethanol, and 60% sucrose, pH 7.2) and (b) 40,000 g for 60 min at 4°C on top of a discontinuous sucrose gradient (40–50–70%, wt/vol). Finally, 12 fractions of 0.1 ml were recovered from the bottom of the tube, and centrosome-containing fractions were identified by Western blot.

Centrosome-associated proteomic analysis

Centrosomes were isolated from resting and activated IIA1.6 cells previously cultured in media containing 1 µg/ml heavy [¹³C⁶] or light [¹²C⁶] L-lysine as previously described (Gogendeau et al., 2015; Obino et al., 2016). Proteins extracted from centrosome-rich fractions were separated on 10% SDS-PAGE gels (Invitrogen) and processed according to the protocol described previously (Obino et al., 2016). The corresponding peptides were extracted and analyzed by nano-liquid chromatography/tandem mass spectrometry using an Ultimate 3000 system (Dionex S.A.) coupled to a LTQ-Orbitrap XL mass spectrometer (Thermo Fisher Scientific). Data were acquired using Xcalibur software (v2.0.7), and the resulting spectra were analyzed via Mascot software (v2.3) with Proteome Discoverer (v1.2; Thermo Fisher Scientific) using the SwissProt *Mus musculus* database (Obino et al., 2016).

Stable isotope labeling with amino acids in cell culture (SILAC)-based protein quantification was performed as previously described (Obino et al., 2016), where peptides extracted ion chromatograms were retrieved from Proteome Discoverer. Scale normalization computed using the package limma from R software was applied to compensate for mixing errors of the

different SILAC cultures as described (Yang et al., 2002). Protein ratios were computed as the geometrical mean of related peptides. To estimate ratio significance, a *t* test was performed with a Benjamini–Hochberg false discovery rate control threshold set to 0.05.

Membrane flotation experiments

Membrane flotation experiments were based on the protocol described by Yeaman (2003) and Yeaman et al. (2004). 10 × 10⁶ cells were seeded in BCR ligand⁺-coated 6-well plates for indicated times, stopping the activation by adding ice-cold PBS. The cells were centrifuged and resuspended in homogenization buffer (20 mM Hepes-KOH, 90 mM KOAc, 2 mM Mg(OAc)₂, and 0.25 M sucrose, pH 7.2). The cell suspension was mechanically lysed through an ice-cold ball-bearing homogenizer. The lysate was centrifuged at 3,000 g, and the supernatant was mixed with iodixanol (Optiprep) to 30% (vol/vol). Lysates were subjected to a discontinuous gradient of 10–20–30% (vol/vol) of iodixanol and centrifuged at 353,000 g for 3 h at 4°C, and the fractions were collected and stored at –80°C.

Synaptic membrane purification

Synaptic membrane isolation was based on the protocol described by Larghi et al. (2013). 5 × 10⁶ B cells were activated in 300 µl of CLICK + 2% FCS containing BCR ligand⁺ Dynabeads (Invitrogen) in a 1:1 ratio (cell/bead) for indicated times. Activation was abruptly stopped by adding 500 µl of ice-cold PBS, and the cells were centrifuged at 600 g for 5 min at 4°C. The cells were resuspended in 500 µl of freeze and thaw buffer (20 mM Tris-HCl, 600 mM KCl, 20% glycerol, 1 mM Na₃VO₄, 5 mM NaF, and protease inhibitors cocktail, pH 7.4) and lysed by seven cycles of freezing and thawing at –80°C. Lysates were incubated for 10 min with Benzonase (Merck) at room temperature followed by 500-µl freeze and thaw buffer washes using a magnet for precipitating the synaptic membrane–Dynabeads complex. Finally, the membrane was resuspended on loading buffer, and fractions were analyzed by Western blot.

Immunoprecipitation of Exo70

10 × 10⁶ IIA1.6 cells were seeded on BCR ligand⁺-coated plates for different times. Activation was stopped by adding cold PBS and then lysed with lysis buffer (25 mM Hepes, pH 7.4, 100 mM KCl, 10 mM MgCl₂, 1% NP-40, 1 mM NaF, 1 mM Na₃VO₄, and protease cocktail inhibitors [Roche]). 800 µg of cell lysate was precleared with protein A-coated agarose beads (Thermo Fisher Scientific) and incubated with Exo70 antibody-coated agarose beads at 4°C overnight. Samples were washed three times with lysis buffer and resuspended in loading buffer.

Western blot

B cells were lysed at 4°C in radioimmunoprecipitation assay buffer supplemented with protease inhibitor cocktail (Roche). Supernatants were collected and loaded onto gels and transferred onto polyvinylidene fluoride membrane (Trans-Blot Semi-Dry Transfer Cell; Bio-Rad). Membranes were blocked in 5% nonfat dry milk resuspended in TBS + 0.05% Tween-20 and incubated overnight at 4°C with primary antibodies, followed

by 60-min incubation with secondary antibodies. Western blots were developed with Westar Supernova substrate (Cyanagen), and chemiluminescence was detected using the G:BOX iChem (Syngene).

Measurement of cell surface levels of BCR by flow cytometry

0.5×10^6 control and Exo70-silenced IIA1.6 cells were incubated on ice for 20 min with PBS plus 3% BSA supplemented with Alexa Fluor 488-conjugated anti-mouse IgG (Thermo Fisher Scientific). Cell surface BCR levels were assessed by flow cytometry (FACSVerse; BD Biosciences).

Statistical analysis

Boxes in box plots extend from the 25th to 75th percentile, with a line at the median and whiskers extending from the 10th to the 90th percentile. Data are generally reported as mean \pm SEM (except when specified) and analyzed by Student's *t* test or one- or two-way ANOVA using GraphPad Prism 5 (GraphPad Software). When using analysis of variance, post hoc analysis was done using Sidak's multiple comparison tests. All statistical analysis was considered significant at $P < 0.05$.

Online supplemental material

Fig. S1 shows the centrosomal localization of exocyst subunits, colocalization analysis of Sec3 and Lamp-1, and a scheme depicting the method used to quantify centrosome polarization to the IS. Fig. S2 shows the localization of endogenous Exo70 in primary B cells, the image analysis of Exo70 recruitment to the IS, and the membrane flotation assay used to characterize the association of Exo70 with membrane fractions in resting and activated B cells. Fig. S3 shows the effect of cytoskeleton-disrupting drugs in B cells, the effect of paclitaxel and SAHA on the microtubule acetylation in B cells, silencing of GEF-H1, and normal polarization of Exo70 to the IS under these conditions. Fig. S4 shows the silencing of Exo70 in B cells, schemes depicting the method used to quantify lysosome distribution, and the effect of Exo70 silencing on surface BCR levels. Fig. S5 shows the silencing Sec3 or Sec8 in B cells and associated functional effects. Video 1 shows TIRF images used to track lysosomes dynamics in control or Exo70-silenced cells.

Acknowledgments

We thank P. Chavrier for providing the Sec3-HA plasmid and M. Bornens for the eGFP-centrin1 plasmid.

M.-I. Yuseff was supported by a research grant from Fondo Nacional de Desarrollo Científico y Tecnológico (#1180900). M.-I. Yuseff, M.R. Bono, and A.-M. Lennon-Duménil were supported by ECOS #C12S02 international research grant. D. Obino was supported by fellowships from the Ecole Doctorale Bio-Sorbonne Paris Cité from the Université Paris Diderot/Université Paris Descartes and the Fondation pour la Recherche Médicale (FDT20150532056). J.J. Sáez and J. Ibañez were supported by fellowships from the Comisión Nacional de Investigación Científica y Tecnológica. This work was supported by the Advanced Microscopy Facility at Pontificia

Universidad Católica de Chile and CONICYT/FONDEQUIP/EQM140016 from Universidad de Chile.

The authors declare no competing financial interests.

Author contributions: J.J. Sáez designed, performed, and analyzed most of the experiments and assembled the figures. J. Diaz performed immunofluorescence and coimmunoprecipitation assays and assisted with experimental setups. J.P. Bozo, F. Cabrera Reyes, and M. Alamo conducted and analyzed immunofluorescence experiments. D. Obino and M.-I. Yuseff contributed to the proteomic analysis of the centrosome in B cells. F.-X. Gobert assisted with the synthesis and infection of viral particles for shRNAs. J. Ibañez analyzed imaging data. C. Yeaman provided tools, protocols, and assistance in biochemical analysis of the exocyst complex. M.R. Bono, A.-M. Lennon-Duménil, and C. Yeaman provided critical feedback for experiments. J.J. Sáez and M.-I. Yuseff wrote the manuscript. M.-I. Yuseff conceived, supervised, and funded the project.

Submitted: 23 November 2018

Revised: 11 April 2019

Accepted: 22 May 2019

References

- Ahmed, S.M., and I.G. Macara. 2017. The Par3 polarity protein is an exocyst receptor essential for mammary cell survival. *Nat. Commun.* 8:14867. <https://doi.org/10.1038/ncomms14867>
- Avalos, A.M., and H.L. Ploegh. 2014. Early BCR events and antigen capture, processing, and loading on MHC class II on B cells. *Front. Immunol.* 5:92. <https://doi.org/10.3389/fimmu.2014.00092>
- Baek, K., A. Knödler, S.H. Lee, X. Zhang, K. Orlando, J. Zhang, T.J. Foscett, W. Guo, and R. Dominguez. 2010. Structure-function study of the N-terminal domain of exocyst subunit Sec3. *J. Biol. Chem.* 285: 10424–10433. <https://doi.org/10.1074/jbc.M109.096966>
- Batista, F.D., and M.S. Neuberger. 2000. B cells extract and present immobilized antigen: implications for affinity discrimination. *EMBO J.* 19: 513–520. <https://doi.org/10.1093/emboj/19.4.513>
- Bendezú, F.O., V. Vincenzetti, and S.G. Martin. 2012. Fission yeast Sec3 and Exo70 are transported on actin cables and localize the exocyst complex to cell poles. *PLoS One*. 7:e40248. <https://doi.org/10.1371/journal.pone.0040248>
- Bhuwania, R., A. Castro-Castro, and S. Linder. 2014. Microtubule acetylation regulates dynamics of KIF1C-powered vesicles and contact of microtubule plus ends with podosomes. *Eur. J. Cell Biol.* 93:424–437. <https://doi.org/10.1016/j.ejcb.2014.07.006>
- Birkenfeld, J., P. Nalbant, S.H. Yoon, and G.M. Bokoch. 2008. Cellular functions of GEF-H1, a microtubule-regulated Rho-GEF: is altered GEF-H1 activity a crucial determinant of disease pathogenesis? *Trends Cell Biol.* 18:210–219. <https://doi.org/10.1016/j.tcb.2008.02.006>
- Birukova, A.A., P. Fu, J. Xing, B. Yakubov, I. Cokic, and K.G. Birukov. 2010. Mechanotransduction by GEF-H1 as a novel mechanism of ventilator-induced vascular endothelial permeability. *Am. J. Physiol. Lung Cell. Mol. Physiol.* 298:L837–L848. <https://doi.org/10.1152/ajplung.00263.2009>
- Bodemann, B.O., A. Orvedahl, T. Cheng, R.R. Ram, Y.H. Ou, E. Formstecher, M. Maiti, C.C. Hazelett, E.M. Wauson, M. Balakireva, et al. 2011. RalB and the exocyst mediate the cellular starvation response by direct activation of autophagosome assembly. *Cell*. 144:253–267. <https://doi.org/10.1016/j.cell.2010.12.018>
- Burbage, M., S.J. Keppler, B. Montaner, P.K. Mattila, and F.D. Batista. 2017. The Small Rho GTPase TC10 Modulates B Cell Immune Responses. *J. Immunol.* 199:1682–1695. <https://doi.org/10.4049/jimmunol.1602167>
- Carrasco, Y.R., S.J. Fleire, T. Cameron, M.L. Dustin, and F.D. Batista. 2004. LFA-1/ICAM-1 interaction lowers the threshold of B cell activation by facilitating B cell adhesion and synapse formation. *Immunity*. 20: 589–599. [https://doi.org/10.1016/S1074-7613\(04\)00105-0](https://doi.org/10.1016/S1074-7613(04)00105-0)
- Chiang, H.S., Y. Zhao, J.H. Song, S. Liu, N. Wang, C. Terhorst, A.H. Sharpe, M. Basavappa, K.L. Jeffrey, and H.C. Reinecker. 2014. GEF-H1 controls

- microtubule-dependent sensing of nucleic acids for antiviral host defenses. *Nat. Immunol.* 15:63–71. <https://doi.org/10.1038/ni.2766>
- Dong, G., A.H. Hutagalung, C. Fu, P. Novick, and K.M. Reinisch. 2005. The structures of exocyst subunit Exo70p and the Exo84p C-terminal domains reveal a common motif. *Nat. Struct. Mol. Biol.* 12:1094–1100. <https://doi.org/10.1038/nsmb1017>
- Dubois, F., K. Alpha, and C.E. Turner. 2017. Paxillin regulates cell polarization and anterograde vesicle trafficking during cell migration. *Mol. Biol. Cell.* 28:3815–3831. <https://doi.org/10.1091/mbc.e17-08-0488>
- Dupraz, S., D. Grassi, M.E. Bernis, L. Sosa, M. Bisbal, L. Gastaldi, I. Jausoro, A. Cáceres, K.H. Pfenniger, and S. Quiroga. 2009. The TC10-Exo70 complex is essential for membrane expansion and axonal specification in developing neurons. *J. Neurosci.* 29:13292–13301. <https://doi.org/10.1523/JNEUROSCI.3907-09.2009>
- Fine, N., I.D. Dimitriou, J. Rullo, M.J. Sandí, B. Petri, J. Haitsma, H. Ibrahim, J. La Rose, M. Glogauer, P. Kubes, et al. 2016. GEF-H1 is necessary for neutrophil shear stress-induced migration during inflammation. *J. Cell Biol.* 215:107–119. <https://doi.org/10.1083/jcb.201603109>
- Fujishiro, S.H., S. Tanimura, S. Mure, Y. Kashimoto, K. Watanabe, and M. Kohno. 2008. ERK1/2 phosphorylate GEF-H1 to enhance its guanine nucleotide exchange activity toward RhoA. *Biochem. Biophys. Res. Commun.* 368:162–167. <https://doi.org/10.1016/j.bbrc.2008.01.066>
- Fujita, A., S. Koinuma, S. Yasuda, H. Nagai, H. Kamiguchi, N. Wada, and T. Nakamura. 2013. GTP hydrolysis of TC10 promotes neurite outgrowth through exocytic fusion of Rab11- and L1-containing vesicles by releasing exocyst component Exo70. *PLoS One.* 8:e79689. <https://doi.org/10.1371/journal.pone.0079689>
- Gogendeau, D., P. Guichard, and A.M. Tassin. 2015. Purification of centrosomes from mammalian cell lines. *Methods Cell Biol.* 129:171–189. <https://doi.org/10.1016/bs.mcb.2015.03.004>
- Grindstaff, K.K., C. Yeaman, N. Anandasabapathy, S.C. Hsu, E. Rodriguez-Boulant, R.H. Scheller, and W.J. Nelson. 1998. Sec6/8 complex is recruited to cell-cell contacts and specifies transport vesicle delivery to the basal-lateral membrane in epithelial cells. *Cell.* 93:731–740. [https://doi.org/10.1016/S0092-8674\(00\)81435-X](https://doi.org/10.1016/S0092-8674(00)81435-X)
- Hamburger, Z.A., A.E. Hamburger, A.P. West Jr., and W.I. Weis. 2006. Crystal structure of the Scervisiae exocyst component Exo70p. *J. Mol. Biol.* 356:9–21. <https://doi.org/10.1016/j.jmb.2005.09.099>
- Harwood, N.E., and F.D. Batista. 2011. The cytoskeleton coordinates the early events of B-cell activation. *Cold Spring Harb. Perspect. Biol.* 3:1–15. <https://doi.org/10.1101/cshperspect.a002360>
- He, B., and W. Guo. 2009. The exocyst complex in polarized exocytosis. *Curr. Opin. Cell Biol.* 21:537–542. <https://doi.org/10.1016/j.ceb.2009.04.007>
- He, B., F. Xi, X. Zhang, J. Zhang, and W. Guo. 2007. Exo70 interacts with phospholipids and mediates the targeting of the exocyst to the plasma membrane. *EMBO J.* 26:4053–4065. <https://doi.org/10.1038/sj.emboj.7601834>
- Heck, J.N., S.M. Ponik, M.G. Garcia-Mendoza, C.A. Pehlke, D.R. Inman, K.W. Eliceiri, and P.J. Keely. 2012. Microtubules regulate GEF-H1 in response to extracellular matrix stiffness. *Mol. Biol. Cell.* 23:2583–2592. <https://doi.org/10.1091/mbc.e11-10-0876>
- Heesters, B.A., C.E. van der Poel, A. Das, and M.C. Carroll. 2016. Antigen Presentation to B Cells. *Trends Immunol.* 37:844–854. <https://doi.org/10.1016/j.it.2016.10.003>
- Heider, M.R., and M. Munson. 2012. Exorcising the Exocyst Complex. *Traffic.* 13:898–907. <https://doi.org/10.1111/j.1600-0854.2012.01353.x>
- Heider, M.R., M. Gu, C.M. Duffy, A.M. Mirza, L.L. Marcotte, A.C. Walls, N. Farrall, Z. Hakhverdyan, M.C. Field, M.P. Rout, et al. 2016. Subunit connectivity, assembly determinants and architecture of the yeast exocyst complex. *Nat. Struct. Mol. Biol.* 23:59–66. <https://doi.org/10.1038/nsmb.3146>
- Jacob, A., D. Cooney, M. Pradhan, and K.M. Coggeshall. 2002. Convergence of signaling pathways on the activation of ERK in B cells. *J. Biol. Chem.* 277:23420–23426. <https://doi.org/10.1074/jbc.M202485200>
- Jenkins, M.R., A. Tsun, J.C. Stinchcombe, and G.M. Griffiths. 2009. The strength of T cell receptor signal controls the polarization of cytotoxic machinery to the immunological synapse. *Immunity.* 31:621–631. <https://doi.org/10.1016/j.immuni.2009.08.024>
- Jones, B., J.P. Tite, and C.A. Janeway Jr. 1986. Different phenotypic variants of the mouse B cell tumor A20/2J are selected by antigen- and mitogen-triggered cytotoxicity of L3T4-positive, I-A-restricted T cell clones. *J. Immunol.* 136:348–356. <http://www.ncbi.nlm.nih.gov/pubmed/2415625>
- Kakiashvili, E., P. Speight, F. Waheed, R. Seth, M. Lodyga, S. Tanimura, M. Kohno, O.D. Rotstein, A. Kapus, and K. Szász. 2009. GEF-H1 mediates tumor necrosis factor- α -induced Rho activation and myosin phosphorylation: role in the regulation of tubular paracellular permeability. *J. Biol. Chem.* 284:11454–11466. <https://doi.org/10.1074/jbc.M805933200>
- Krendel, M., F.T. Zenke, and G.M. Bokoch. 2002. Nucleotide exchange factor GEF-H1 mediates cross-talk between microtubules and the actin cytoskeleton. *Nat. Cell Biol.* 4:294–301. <https://doi.org/10.1038/ncb773>
- Lankar, D., H. Vincent-Schneider, V. Briken, T. Yokozeki, G. Raposo, and C. Bonnerot. 2002. Dynamics of major histocompatibility complex class II compartments during B cell receptor-mediated cell activation. *J. Exp. Med.* 195:461–472. <https://doi.org/10.1084/jem.20011543>
- Larghi, P., D.J. Williamson, J.-M. Carpié, S. Dogniaux, K. Chemin, A. Bohineust, L. Danglot, K. Gaus, T. Galli, and C. Hivroz. 2013. VAMP7 controls T cell activation by regulating the recruitment and phosphorylation of vesicular Lat at TCR-activation sites. *Nat. Immunol.* 14:723–731. <https://doi.org/10.1038/ni.2609>
- Le Roux, D., D. Lankar, M.-I. Yuseff, F. Vascotto, T. Yokozeki, G. Faure-André, E. Mougneau, N. Glaichenhaus, B. Manoury, C. Bonnerot, and A.-M. Lennon-Duménil. 2007. Syk-dependent actin dynamics regulate endocytic trafficking and processing of antigens internalized through the B-cell receptor. *Mol. Biol. Cell.* 18:3451–3462. <https://doi.org/10.1091/mbc.e06-12-1114>
- Lin, K.B.L., S.A. Freeman, S. Zabetian, H. Brugger, M. Weber, V. Lei, M. Dang-Lawson, K.W.K. Tse, R. Santamaria, F.D. Batista, and M.R. Gold. 2008. The rap GTPases regulate B cell morphology, immune-synapse formation, and signaling by particulate B cell receptor ligands. *Immunity.* 28:75–87. <https://doi.org/10.1016/j.immuni.2007.11.019>
- Lipschutz, J.H., W. Guo, L.E. O'Brien, Y.H. Nguyen, P. Novick, and K.E. Mostov. 2000. Exocyst is involved in cystogenesis and tubulogenesis and acts by modulating synthesis and delivery of basolateral plasma membrane and secretory proteins. *Mol. Biol. Cell.* 11:4259–4275. <https://doi.org/10.1091/mbc.11.12.4259>
- Liu, J., X. Zuo, P. Yue, and W. Guo. 2007. Phosphatidylinositol 4,5-bisphosphate mediates the targeting of the exocyst to the plasma membrane for exocytosis in mammalian cells. *Mol. Biol. Cell.* 18:4483–4492. <https://doi.org/10.1091/mbc.e07-05-0461>
- Liu, J., P. Yue, V.V. Artym, S.C. Mueller, and W. Guo. 2009. The role of the exocyst in matrix metalloproteinase secretion and actin dynamics during tumor cell invadopodia formation. *Mol. Biol. Cell.* 20:3763–3771. <https://doi.org/10.1091/mbc.e08-09-0967>
- Liu, J., Y. Zhao, Y. Sun, B. He, C. Yang, T. Svitkina, Y.E. Goldman, and W. Guo. 2012. Exo70 stimulates the Arp2/3 complex for lamellipodia formation and directional cell migration. *Curr. Biol.* 22:1510–1515. <https://doi.org/10.1016/j.cub.2012.05.055>
- Ma, W., Y. Wang, X. Yao, Z. Xu, L. An, and M. Yin. 2016. The role of Exo70 in vascular smooth muscle cell migration. *Cell. Mol. Biol. Lett.* 21:20. <https://doi.org/10.1186/s11658-016-0019-8>
- Malherbe, L., C. Filippi, V. Julia, G. Foucras, M. Moro, H. Appel, K. Wucherpfennig, J.C. Guéry, and N. Glaichenhaus. 2000. Selective activation and expansion of high-affinity CD4⁺ T cells in resistant mice upon infection with Leishmania major. *Immunity.* 13:771–782. [https://doi.org/10.1016/S1074-7613\(00\)00075-3](https://doi.org/10.1016/S1074-7613(00)00075-3)
- Mattila, P.K., C. Feest, D. Depoil, B. Treanor, B. Montaner, K.L. Otipoby, R. Carter, L.B. Justement, A. Bruckbauer, and F.D. Batista. 2013. The actin and tetraspanin networks organize receptor nanoclusters to regulate B cell receptor-mediated signaling. *Immunity.* 38:461–474. <https://doi.org/10.1016/j.immuni.2012.11.019>
- Meiri, D., C.B. Marshall, M.A. Greeve, B. Kim, M. Balan, F. Suarez, C. Bakal, C. Wu, J. Larose, N. Fine, et al. 2012. Mechanistic insight into the microtubule and actin cytoskeleton coupling through dynein-dependent RhoGEF inhibition. *Mol. Cell.* 45:642–655. <https://doi.org/10.1016/j.molcel.2012.01.027>
- Milasta, S., N.A. Evans, L. Ormiston, S. Wilson, R.J. Lefkowitz, and G. Milligan. 2005. The sustainability of interactions between the orexin-1 receptor and beta-arrestin-2 is defined by a single C-terminal cluster of hydroxy amino acids and modulates the kinetics of ERK MAPK regulation. *Biochem. J.* 387:573–584. <https://doi.org/10.1042/BJ20041745>
- Mitchison, N.A. 2004. T-cell-B-cell cooperation. *Nat. Rev. Immunol.* 4:308–312. <https://doi.org/10.1038/nri1334>
- Mohammadi, S., and R.R. Isberg. 2013. Cdc42 interacts with the exocyst complex to promote phagocytosis. *J. Cell Biol.* 200:81–93. <https://doi.org/10.1083/jcb.201204090>
- Moore, B.A., H.H. Robinson, and Z. Xu. 2007. The crystal structure of mouse Exo70 reveals unique features of the mammalian exocyst. *J. Mol. Biol.* 371:410–421. <https://doi.org/10.1016/j.jmb.2007.05.018>

- Morgera, F., M.R. Sallah, M.L. Dubuke, P. Gandhi, D.N. Brewer, C.M. Carr, and M. Munson. 2012. Regulation of exocytosis by the exocyst subunit Sec6 and the SM protein Sec1. *Mol. Biol. Cell.* 23:337–346. <https://doi.org/10.1091/mbc.e11-08-0670>
- Natkanski, E., W. Lee, B. Mistry, A. Casal, J.E. Molloy, and P. Tolar. 2013. B cells use mechanical energy to discriminate antigen affinities. *Science*. 340:1587–1590. <https://doi.org/10.1126/science.1237572>
- Novick, P., C. Field, and R. Schekman. 1980. Identification of 23 complementation groups required for post-translational events in the yeast secretory pathway. *Cell*. 21:205–215. [https://doi.org/10.1016/0092-8674\(80\)90128-2](https://doi.org/10.1016/0092-8674(80)90128-2)
- Obino, D., F. Farina, O. Malbec, P.J. Sáez, M. Maurin, J. Gaillard, F. Dingli, D. Loew, A. Gautreau, M.-I. Yuseff, et al. 2016. Actin nucleation at the centrosome controls lymphocyte polarity. *Nat. Commun.* 7:10969. <https://doi.org/10.1038/ncomms10969>
- Obino, D., J. Díaz, J.J. Sáez, J. Ibañez-Vega, P.J. Sáez, M. Alamo, D. Lankar, and M.-I. Yuseff. 2017. Vamp-7-dependent secretion at the immune synapse regulates antigen extraction and presentation in B-lymphocytes. *Mol. Biol. Cell*. 28:890–897. <https://doi.org/10.1091/mbc.e16-10-0722>
- Orange, J.S. 2008. Formation and function of the lytic NK-cell immunological synapse. *Nat. Rev. Immunol.* 8:713–725. <https://doi.org/10.1038/nri2381>
- Oztan, A., M. Silvis, O.A. Weisz, N.A. Bradbury, S.-C. Hsu, J.R. Goldenring, C. Yeaman, and G. Apodaca. 2007. Exocyst requirement for endocytic traffic directed toward the apical and basolateral poles of polarized MDCK cells. *Mol. Biol. Cell*. 18:3978–3992. <https://doi.org/10.1091/mbc.e07-02-0097>
- Pathak, R., and C. Dermardirossian. 2013. GEF-H1: orchestrating the interplay between cytoskeleton and vesicle trafficking. *Small GTPases*. 4:174–179. <https://doi.org/10.4161/sgtp.24616>
- Pathak, R., V.D. Delorme-Walker, M.C. Howell, A.N. Anselmo, M.A. White, G.M. Bokoch, and C. Dermardirossian. 2012. The microtubule-associated Rho activating factor GEF-H1 interacts with exocyst complex to regulate vesicle traffic. *Dev. Cell*. 23:397–411. <https://doi.org/10.1016/j.devcel.2012.06.014>
- Polgar, N., and B. Fogelgren. 2018. Regulation of Cell Polarity by Exocyst-Mediated Trafficking. *Cold Spring Harb. Perspect. Biol.* 10:a031401. <https://doi.org/10.1101/cshperspect.a031401>
- Pommereit, D., and F.S. Wouters. 2007. An NGF-induced Exo70-TC10 complex locally antagonises Cdc42-mediated activation of N-WASP to modulate neurite outgrowth. *J. Cell Sci.* 120:2694–2705. <https://doi.org/10.1242/jcs.03475>
- Reversat, A., M.-I. Yuseff, D. Lankar, O. Malbec, D. Obino, M. Maurin, N.V.G. Penmarcha, A. Amoroso, L. Sengmanivong, G.G. Gundersen, et al. 2015. Polarity protein Par3 controls B-cell receptor dynamics and antigen extraction at the immune synapse. *Mol. Biol. Cell*. 26:1273–1285. <https://doi.org/10.1091/mbc.E14-09-1373>
- Sánchez-Ruiz, J., R. Mejías, M. García-Belando, D.F. Barber, and A. González-García. 2011. Ral GTPases regulate cell-mediated cytotoxicity in NK cells. *J. Immunol.* 187:2433–2441. <https://doi.org/10.4049/jimmunol.1003089>
- Schindelin, J., I. Arganda-Carreras, E. Frise, V. Kaynig, M. Longair, T. Pietzsch, S. Preibisch, C. Rueden, S. Saalfeld, B. Schmid, et al. 2012. Fiji: an open-source platform for biological-image analysis. *Nat. Methods*. 9: 676–682. <https://doi.org/10.1038/nmeth.2019>
- Shen, D., H. Yuan, A. Hutagalung, A. Verma, D. Kümmel, X. Wu, K. Reinisch, J.A. McNean, and P. Novick. 2013. The synaptobrevin homologue Snc2p recruits the exocyst to secretory vesicles by binding to Sec6p. *J. Cell Biol.* 202:509–526. <https://doi.org/10.1083/jcb.201211148>
- Spiczka, K.S., and C. Yeaman. 2008. Ral-regulated interaction between Sec5 and paxillin targets Exocyst to focal complexes during cell migration. *J. Cell Sci.* 121:2880–2891. <https://doi.org/10.1242/jcs.031641>
- Stinchcombe, J.C., and G.M. Griffiths. 2007. Secretory mechanisms in cell-mediated cytotoxicity. *Annu. Rev. Cell Dev. Biol.* 23:495–517. <https://doi.org/10.1146/annurev.cellbio.23.090506.123521>
- Stinchcombe, J.C., G. Bossi, S. Booth, and G.M. Griffiths. 2001. The immunological synapse of CTL contains a secretory domain and membrane bridges. *Immunity*. 15:751–761. [https://doi.org/10.1016/S1074-7613\(01\)00234-5](https://doi.org/10.1016/S1074-7613(01)00234-5)
- Stinchcombe, J.C., E. Majorovits, G. Bossi, S. Fuller, and G.M. Griffiths. 2006. Centrosome polarization delivers secretory granules to the immunological synapse. *Nature*. 443:462–465. <https://doi.org/10.1038/nature05071>
- TerBush, D.R., T. Maurice, D. Roth, and P. Novick. 1996. The Exocyst is a multiprotein complex required for exocytosis in *Saccharomyces cerevisiae*. *EMBO J.* 15:6483–6494. <https://doi.org/10.1002/j.1460-2075.1996.tb01039.x>
- Thapa, N., Y. Sun, M. Schram, S. Choi, K. Ling, and R.A. Anderson. 2012. Phosphoinositide signaling regulates the exocyst complex and polarized integrin trafficking in directionally migrating cells. *Dev. Cell*. 22:116–130. <https://doi.org/10.1016/j.devcel.2011.10.030>
- Treanor, B., D. Depoil, A. Gonzalez-Granja, P. Barral, M. Weber, O. Dushek, A. Bruckbauer, and F.D. Batista. 2010. The membrane skeleton controls diffusion dynamics and signaling through the B cell receptor. *Immunity*. 32:187–199. <https://doi.org/10.1016/j.immuni.2009.12.005>
- Vascotto, F., D. Lankar, G. Faure-André, P. Vargas, J. Diaz, D. Le Roux, M.I. Yuseff, J.B. Sibarita, M. Boes, G. Raposo, et al. 2007. The actin-based motor protein myosin II regulates MHC class II trafficking and BCR-driven antigen presentation. *J. Cell Biol.* 176:1007–1019. <https://doi.org/10.1083/jcb.200611147>
- Wang, S., Y. Liu, C.L. Adamson, G. Valdez, W. Guo, and S.C. Hsu. 2004. The mammalian exocyst, a complex required for exocytosis, inhibits tubulin polymerization. *J. Biol. Chem.* 279:35958–35966. <https://doi.org/10.1074/jbc.M313778200>
- Westermann, S., and K. Weber. 2003. Post-translational modifications regulate microtubule function. *Nat. Rev. Mol. Cell Biol.* 4:938–947. <https://doi.org/10.1038/nrml260>
- Wu, B., and W. Guo. 2015. The Exocyst at a Glance. *J. Cell Sci.* 128:2957–2964. <https://doi.org/10.1242/jcs.156398>
- Yamamoto, A., A. Kasamatsu, S. Ishige, K. Koike, K. Saito, Y. Kouzu, H. Koike, Y. Sakamoto, K. Ogawara, M. Shiiba, et al. 2013. Exocyst complex component Sec8: a presumed component in the progression of human oral squamous-cell carcinoma by secretion of matrix metalloproteinases. *J. Cancer Res. Clin. Oncol.* 139:533–542. <https://doi.org/10.1007/s00432-012-1356-2>
- Yang, Y.H., S. Dudoit, P. Luu, D.M. Lin, V. Peng, J. Ngai, and T.P. Speed. 2002. Normalization for cDNA microarray data: a robust composite method addressing single and multiple slide systematic variation. *Nucleic Acids Res.* 30:e15. <https://doi.org/10.1093/nar/30.4.e15>
- Yeaman, C. 2003. Ultracentrifugation-based approaches to study regulation of Sec6/8 (exocyst) complex function during development of epithelial cell polarity. *Methods*. 30:198–206. [https://doi.org/10.1016/S1046-2023\(03\)00026-4](https://doi.org/10.1016/S1046-2023(03)00026-4)
- Yeaman, C., K.K. Grinstead, and W.J. Nelson. 2004. Mechanism of recruiting Sec6/8 (exocyst) complex to the apical junctional complex during polarization of epithelial cells. *J. Cell Sci.* 117:559–570. <https://doi.org/10.1242/jcs.00893>
- Yue, P., Y. Zhang, K. Mei, S. Wang, J. Lesigang, Y. Zhu, G. Dong, and W. Guo. 2017. Sec3 promotes the initial binary t-SNARE complex assembly and membrane fusion. *Nat. Commun.* 8:14236. <https://doi.org/10.1038/ncomms14236>
- Yuseff, M.I., and A.M. Lennon-Dumenil. 2013. Studying MHC class II presentation of immobilized antigen by B lymphocytes. *Methods Mol. Biol.* 960:529–543. https://doi.org/10.1007/978-1-62703-218-6_39
- Yuseff, M.I., A. Reversat, D. Lankar, J. Diaz, I. Fanget, P. Pierobon, V. Randrian, N. Larochette, F. Vascotto, C. Desdouets, et al. 2011. Polarized secretion of lysosomes at the B cell synapse couples antigen extraction to processing and presentation. *Immunity*. 35:361–374. <https://doi.org/10.1016/j.immuni.2011.07.008>
- Yuseff, M.-I., P. Pierobon, A. Reversat, and A.-M. Lennon-Duménil. 2013. How B cells capture, process and present antigens: a crucial role for cell polarity. *Nat. Rev. Immunol.* 13:475–486. <https://doi.org/10.1038/nri3469>
- Zeng, J., S. Feng, B. Wu, and W. Guo. 2017. Polarized Exocytosis. *Cold Spring Harb. Perspect. Biol.* 9:a027870. <https://doi.org/10.1101/cshperspect.a027870>
- Zhang, X., K. Orlando, B. He, F. Xi, J. Zhang, A. Zajac, and W. Guo. 2008. Membrane association and functional regulation of Sec3 by phospholipids and Cdc42. *J. Cell Biol.* 180:145–158. <https://doi.org/10.1083/jcb.200704128>
- Zhang, Y., N. Li, C. Caron, G. Matthias, D. Hess, S. Khochbin, and P. Matthias. 2003. HDAC-6 interacts with and deacetylates tubulin and microtubules in vivo. *EMBO J.* 22:1168–1179. <https://doi.org/10.1093/emboj/cdg115>
- Zuo, X., J. Zhang, Y. Zhang, S.-C. Hsu, D. Zhou, and W. Guo. 2006. Exo70 interacts with the Arp2/3 complex and regulates cell migration. *Nat. Cell Biol.* 8:1383–1388. <https://doi.org/10.1038/ncb1505>